university of groningen / faculty of science and engineering

Bachelor Integration Project

Report

Performance Prediction in Offshore Wind Farms: Modeling Hollandse Kust Noord

Author:
Anouk Werre (s4833872)

1st Supervisor:
Prof. Dr. A. Vakis
2nd Supervisor:
M. Mohebbi
Company Supervisor:
R. Nienhuis

Groningen, January 27, 2025

BSc. Industrial Engineering and Management
Faculty of Science and Engineering
University of Groningen

Abstract

The Netherlands aims to achieve a fully sustainable energy system by 2050, with offshore wind energy as a key contributor due to favorable North Sea conditions. However, wind energy's intermittency creates challenges like overproduction during low demand and underproduction during high demand, highlighting the potential of energy storage systems (ESS). This research develops an offshore wind farm model using the SIMSEN software, including realistic conditions such as wake effects and wind variability of an existing wind farm in the North Sea (Hollandse Kust Noord). The model provides insights into wind farm performance and lays the ground work for future studies on ESS integration to enhance grid stability and optimize wind farm operations through the SIMSEN software.

Contents

1 Acronyms

Acronym	Definition
BaIP	Bachelor Integration Project
ESS	Energy Storage System
HKN	Hollandse Kust Noord
RDP	Research Design Plan
ROM	Reduced Order Modeling
RSS	Root Sum of Squares
SG	Siemens Gamesa
SW	South-West
TSR	Tip Speed Ratio
WT	Wind Turbine

2 Introduction

As the world shifts towards a more sustainable future, renewable energy sources play a key role in reducing reliance on fossil fuels. The Netherlands has set a goal to rely entirely on sustainable energy by 2050, with wind energy expected to be the largest contributor. This is partly due to the Netherlands' location on the North Sea, which provides favorable conditions for offshore wind energy generation [1].

Offshore wind turbines take advantage of stronger winds at sea [2]. However, wind energy is intermittent, meaning power generation fluctuates with wind speed patterns. This intermittency brings challenges to grid stability and energy reliability. For instance, during periods of high wind speeds and low electricity demand, energy that is overproduced often leads to curtailment whereby valuable energy is wasted. During periods of low wind speeds and high electricity demand, backup generation is needed which often relies on fossil fuels [3].

Integrating energy storage systems (ESS) offers a promising solution to this waste of renewable energy. ESS could store energy resulting from overproduction during high wind periods, and release this energy when the demand is high while there is a low wind period. The process of storing surplus energy can help to reduce power fluctuations, improves the reliability of energy supply, and thereby reduces the need for curtailment. Thus, ESS can make offshore wind farms operate more efficiently and improve their overall economic performance [4, 5, 6, 7].

Accurate modeling of wind farms is crucial for evaluating the impact of systems like ESS. A key challenge is capturing the complexity of turbine interactions, including wake effects that affect the energy output of downstream turbines and the variability in wind profiles that influences overall performance [8, 9, 10]. Realistic operational and environmental conditions are required for effectively modeling wind variability and wake effects. Once a precise model is created, it can be used to analyze key performance metrics, such as energy efficiency, velocity deficits and power outputs, under existing grid conditions. These insights will enhance the understanding of wind farm performance [11].

Despite existing research on wind turbine modeling, no previous studies were found that focused on modeling an existing offshore wind farm location in the North Sea. This gap in the literature led to the decision to model Hollandse Kust Noord (HKN) as the case study for this research. The SIMSEN software provides a base model for individual wind turbines, and research has explored the modeling of an offshore wind farms in SIMSEN [12]. SIMSEN is a well-suited simulation software for modeling systems involving mechanical, electrical, and hydraulic components and simulates dynamic behavior by using differential-algebraic equations [13]. Existing SIMSEN elements and models will be used and adapted to reflect realistic conditions specific to the HKN site.

The main objective of this Bachelor Integration Project (BaIP) is to lay the groundwork for accurately modeling a specific offshore wind farm using SIMSEN, based on data from the HKN location in the North Sea. While the model developed in this project is not yet fully accurate, it serves as an important step towards predicting the power output for this particular wind farm. Future research will build upon this work, eventually enabling the integration of ESS into the model to assess their impact on grid stability, intermittency, and offshore wind farm operations.

3 Research Design

Section 3 describes the general set-up of this research. Firstly, a problem analysis is provided from which it becomes clear what the actual problem is. Based on this, a problem statement and goal statement are formulated. This section is finalized by an outline for the remainder of the research.

3.1 Problem Context

Wind turbines consist of two primary subsystems which are the mechanical and electrical subsystem. In the mechanical subsystem, the rotor of the turbine captures the kinetic energy from the wind and converts it into mechanical energy by the rotation of the blades and hub. In the electrical system, the rotor of the generator converts the mechanical energy delivered by the turbine into electrical energy using electromagnetic induction [14, 15].

For modeling and assessing wake effects, both the hydraulic and mechanical domain should be taken into account. The hydraulic domain falls under the fluid flow dynamics which in this case involves the wind flow. As wind flows through a turbine, the turbine extracts kinetic energy, causing the wind speed to decrease in the wake region behind it. This also leads to a significant pressure drop at the turbine, which will recover as the wake moves downstream. The wind outside this wake, flowing faster than the wind inside the wake, will interact with the slower moving wake wind, forming a shear layer. Within this layer, turbulence is generated, which causes the external air flow to be mixed with the air within the wake. Mixing this air adds momentum from the external air to the wake, helping the wake to recover some of its speed as it moves downstream [16, 17, 18, 19, 20].

The mechanical domain includes the interaction of these fluid flow dynamics with the mechanical system of the wind turbine. Here, it is examined how the turbulence and influenced wind speeds affect the turbine structure, blades and performance. Turbines, that are located in the wake area of upstream turbines, experience increased fatigue loads due to these effects. Consequently, this will reduce the power output and affects the economic benefits and safe operation of the entire farm [16, 21].

Accurately modeling offshore wind farms under site-specific conditions, accounting for realistic wake effects and wind variability, remains an ongoing challenge in renewable energy research. Wakes are one of the main factors affecting the capacity and efficiency of wind farms, making wake modeling a critical element in performance prediction [22]. The constantly changing wind pattern variations are highly unpredictable and even the slightest differences in wind speed or direction can significantly impact the way turbines interact [23, 17]. When wind direction slightly shifts, the wake generated by one turbine may affect downstream turbines differently, changing their power output and efficiency to decrease. Similarly, fluctuating wind speeds and directions influence the wake recovery process, further complicating the accurate prediction of turbine performance within the wind farm.

In conclusion, understanding and accurately modeling wake effects and their interaction with both the hydrodynamic and mechanical domains is essential for assessing and predicting the performance and reliability of offshore wind farms. This integration is key to improving turbine efficiency, ensuring safe operation, and maximizing the economic viability of renewable energy systems.

3.2 Why-What Analysis

A why-what model is shown in fig 1 which highlights the underlying problem for this research. In the middle block the problem is stated which is that a precise and comprehensive model of

an existing offshore wind farm, considering realistic operational and environmental conditions is currently lacking in SIMSEN. This results in the question of 'why do we want to solve this problem?'. First of all, this accurate model needs to be created in order to ensure accurate performance prediction. Secondly, the goal is to analyze key performance metrics to better understand the efficiency and eventually create a system that can be integrated with an ESS. The question 'What is stopping us from solving this problem?' can be divided into two parts. First of all, models that capture the variability in wind farm performance are currently not available in SIMSEN. Secondly, the reason why these models are incomplete is that the complexity of wind farm modeling is high due to environmental factors, wake effects, and turbine interactions.

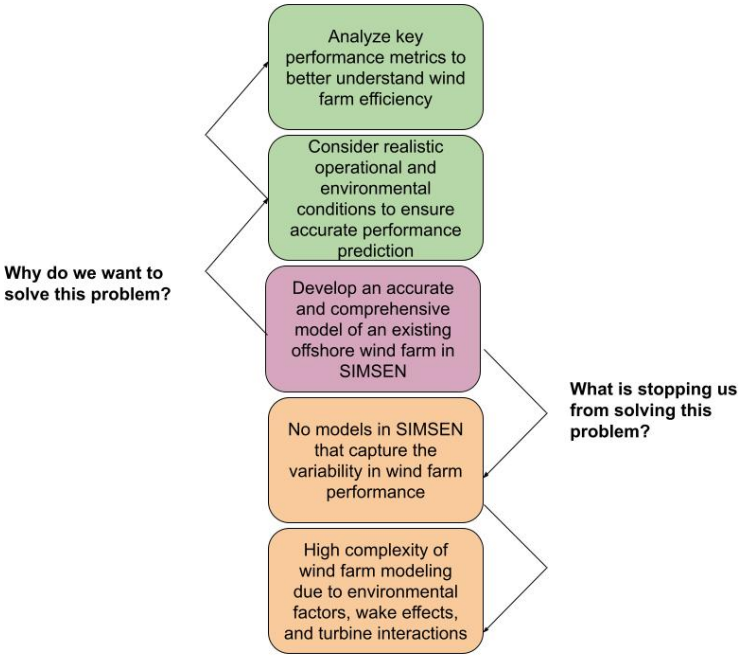

Figure 1: Why-What Model capturing the main problem (red), why we want to solve the problem (green) and what is stopping us from solving the problem (orange)

3.3 Problem Statement

The intermittent nature of offshore wind energy, in combination with the complexity of wind turbine interactions and wake effects, necessitates the development of accurate wind farm models to enhance performance analysis and enable future integration of energy storage systems for improved grid stability.

3.4 Research Goal

The goal of this research is to build and test a working model of an existing offshore wind farm in the North Sea, HKN, using the SIMSEN software by the end of this BaIP. The model will include site-specific wind conditions and turbine setups to simulate energy production and wake effects. The results of this research will lay the groundwork for future integration with Energy Storage Solutions (ESS). However, significant adjustments to the model will still be required before it can be integrated with ESS and used to analyze their impact on offshore wind farms.

3.5 Research Question

The central research question of this BaIP is:

How can the HKN offshore wind farm be modeled in SIMSEN to assess wake effects and turbine performance under site-specific wind conditions, including fluctuating wind speeds and directions, for accurate performance prediction?

3.6 Software Tool

For this BaIP, the simulation software SIMSEN was used, which enables to model and analyze complex energy systems involving mechanical, electrical, and hydraulic components [24]. SIMSEN is effective in studying dynamic behaviors such as energy generation, storage, and grid interactions. Its ability to include site-specific conditions such as wind patterns makes it highly suitable for renewable energy applications, including wind farms.

The software relies on a reduced-order modeling (ROM) approach, which simplifies complex systems while maintaining acceptable accuracy. By using differential-algebraic equations, SIMSEN can simulate dynamic behaviors efficiently [13].

3.7 BaIP Outline

First of all, section 4 provides an introduction to the single wind turbine behavior, wake effects, and wake effect models. Section 5 will provide all formulas necessary for modeling a single wind turbine in SIMSEN. Section 6 explains the setup and elements used of the simulation software SIMSEN. Section 7 introduces the necessary information about HKN and explains the different case scenarios that have been developed for examining the influence of changes in wind speeds and directions. Section 8 will explain all assumptions and key considerations that have been made for modeling HKN in SIMSEN. Section 9 covers all results that were obtained for modeling the lower section of HKN where the influence of wake effects for two case scenarios will be compared. In section 10 it is explained how the model created in SIMSEN has been validated. This BaIP is concluded by interpretation of the model results, and recommendations for future research are provided in section 11. Last, in section 12 the goal of this research will be reflected and a final conclusion is given.

4 Literature Review

Section 4 further elaborates on the key parameters and variables that are required for effectively modeling wind turbines in SIMSEN. It will first explain the affect of increasing wind speeds on the turbine behavior. Then, wake effect models will be introduced.

4.1 Operational Regions of a Wind Turbine

It is important to understand how a single wind turbine behaves at steady-state for different incoming wind speeds in order to accurately model the system. This section includes the key parameters that need to be correctly modeled for accurately modeling a single wind turbine. Different controls can be used for limiting or regulating the power output of wind turbines, which is highly important as turbines are completely dependent on wind flow for generating power. The two main controls are a blade pitch controller and a generator torque controller [25].

The generator torque controller is designed to maximize power extraction below rated wind speeds. It important to know the distinction between the aerodynamic torque and generator torque for this matter. Aerodynamic torque drives the rotor and is generated by the wind acting on the blades of the turbine. It results from the aerodynamic lift and drag forces produced as the wind passes over the blades, and acts as an accelerating load. In the contrary, the generator torque acts as a braking load applied by the generator as it converts the mechanical energy from the rotor into electrical energy.

The second control is a blades collective pitch controller which is designed to regulate rotor and generator speed above rated wind speed. These two controls are applied across four distinct operational regions: I, II, III, and IV (see Fig. 2) [26, 27, 28]

In region I, where wind speeds are lower than the cut-in wind speed and therefore the turbine doesn't generate power. The cut-in wind speed is usually set at 3 or 4 m/s. The generator torque is set to zero in this region to allow the rotor to accelerate without extracting power, preparing the turbine for start-up. The blade pitch angle is set to zero in this region, causing the blades to capture the most possible energy coming from the incoming wind flow [26, 27].

In region II, between the cut-in wind speed and rated wind speed, the main goal is to maximize power extraction. Here, the tip speed ratio (TSR) is kept constant at its optimal value, meaning that the rotor speed increases proportionally with wind speed. This optimal TSR creates the optimal power coefficient. Keeping the TSR constant at its optimal value is achieved by adjusting the generator torque to be proportional to the square of the rotor speed. Furthermore, rotor speed is bounded by a lower and upper limit as a turbine can only operate within these rotor limits. The turbine operates at its specified TSR until either rated power or the maximum rotor speed is reached. The pitch angle is still set to zero in this region to capture the highest amount of wind energy [26, 27].

In region III, above rated wind speeds, the rotor speed exceeds its rated condition. Here, the generator torque is kept constant at its rated value and the pitch angle is adjusted to maintain rotor speed at its rated value and thereby protect the turbine from potential damage. The power output of the system is now maximized to its rated value.

In region IV, wind speeds exceed the cut-out wind speed, which is the maximum wind speed for safe turbine operation. Here, the turbine is automatically shut off [26, 27]. The different regions are shown in Figure 2.

As the generator torque corresponds to the electrical subsystem of the turbine which is outside the scope of this research, aerodynamic constraints will be added to the model. These constraints will ensure that the turbine maintains a constant TSR, as well as a defined minimum and maximum

rotor speed. The methodology for adding these constraints to the model is further explained in Section 5.

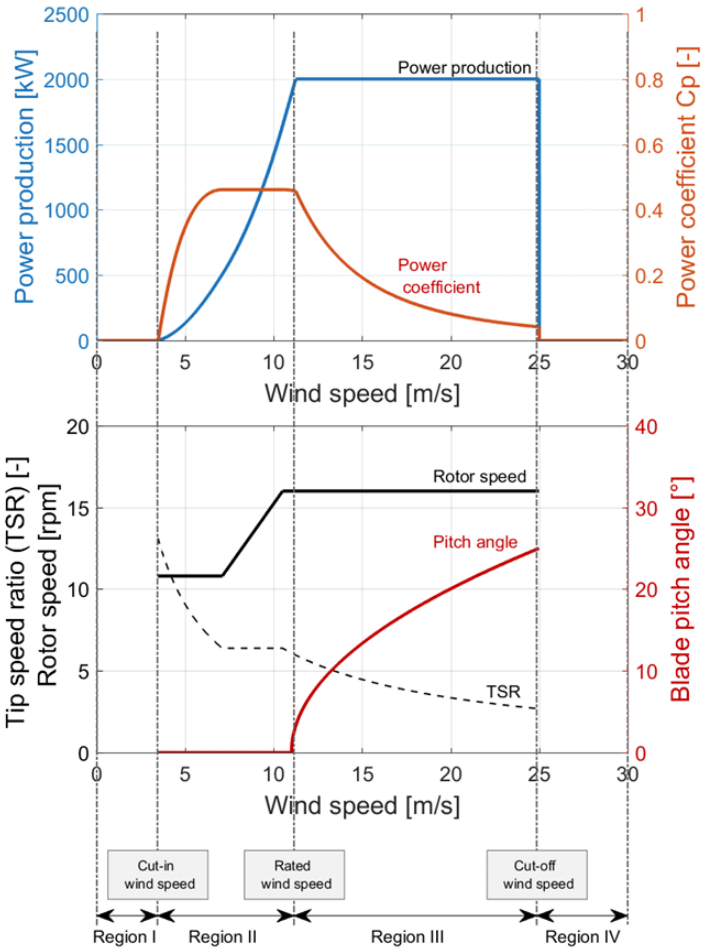

Figure 2: Operational Regions of a Wind Turbine in Steady-State [27]

4.2 Wake Effects

When designing a wind farm, the primary objective is to maximize energy output using the fewest turbines and the least amount of space. The wake effect refers to the region of altered airflow that forms downstream of a wind turbine as a result of energy extraction from the wind by the turbine rotor. The wake created by a single turbine can be divided into two regions: the near wake and the far wake.

The near wake region extends approximately 2–4 rotor diameters downstream of the turbine [20] [29] [17] [30]. In this region, the wind flow is highly influenced by the geometry of the rotor resulting in high-pressure air on the upstream side of the blades moving to the low-pressure side, creating tip vortices [17]. These significant changes in pressure and wind speed lead to the expansion of the wake. As the fluid moves downstream and and returns to atmospheric pressure, the velocity deficit in the wake region reaches it maximum value. This point represents the transition from the near wake region to the far wake region [16].

In the far wake region, the primary factor becomes turbulence and the impact of the rotor on the wind flow decreases. Atmospheric turbulence mixes with turbulence generated by the rotor, speeding up the recovery of the wake where wind speeds deficits are reduced as explained in Section 3.1. The layout of a wind farm is crucial to minimizing these impacts, as changes in wind

direction or wake interactions directly affect the wind farm's overall performance [11]. Figure 3 provides a visual representation of the wake effect between upstream and downstream turbines.

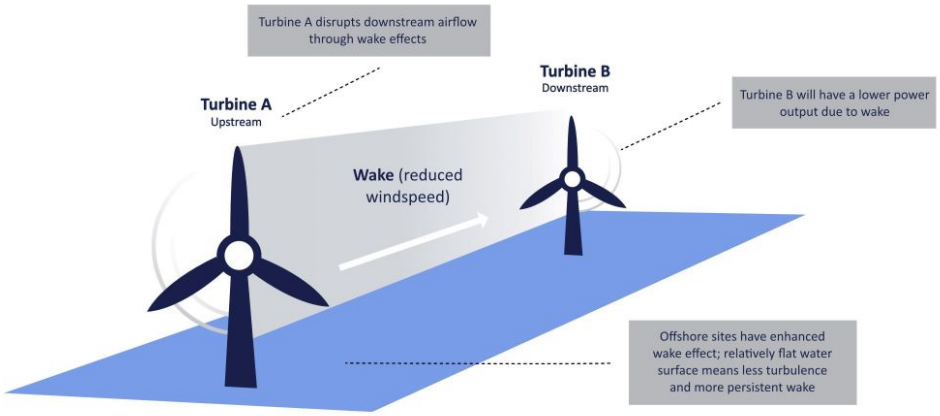

Figure 3: Wake Effect on Downstream Wind Turbine

4.3 Wake Models

There are many different models available in literature for assessing the impact of wake effects on velocity deficits and energy yields. These wake models have been categorized in 1D and 2D models. Examples of 1D models are Jensen's model, Frandsen's model, Larsen's model, and Ishihara's model to name a few. All these 1D models have in common that they assume a linear expansion of velocity profiles, which can lead to overestimated wind speeds in the wake [31, 32]. While this assumption does not perfectly align with the complexity of real world wind patterns, these 1D models still provide useful approximations in many contexts.

Among these 1D models, the Jensen's model is most widely used in academic research due to its computational efficiency and simplicity [30, 33, 10, 34]. Despite its top-hat distribution shape and constant wake decay parameter, it remains a valuable tool as its prediction accuracy is still within an acceptable degree [20, 35].

Jensen's 1D model has one other key limitation. The second key limitation is the assumption of a constant wake decay parameter through the entire wake flow field [36]. This wake decay coefficient denoted as k [-], describes the rate at which the wake expands when traveling downstream.

For more precise modeling, 2D wake models are often preferred. These models improve the 1D models by offering a more realistic representation of velocity deficits using Gaussian of trigonometric distributions (see Figure 4) [31, 30, 19, 35]. Literature has introduced multiple 2D wake effect models that represent important extensions to Jensen's 1D model, such as the 2D Jensen, 2Dk Jensen, and Jensen-Gaussian model. These models include more realistic wind velocity profiles and turbulence by making the following adjustments. Jensen's 2D wake model replaces the simplistic top-hat velocity deficit profile with a more realistic cosine-shaped distribution. Jensen's 2Dk model further modifies the wake decay parameter to account for both ambient turbulence and wake-generated turbulence, as well as the downstream distance from the turbine. The 2D Jensen-Gaussian model is an extension that combines Jensen's 1D model with a Gaussian distribution [37].

While these 2D models are better suited for more accurate predictions of wake dynamics, Jensen's 1D wake model remains a reliable starting point for understanding wake effects [20, 35]. Currently,

no explicit publications have been found in literature that address turbine interactions in detail at the HKN. In this case, Jensen's 1D model provides a useful way to estimate the influence of each turbine on downstream turbines by its linear wake expansion. Even though it may overestimate velocity deficits, this model is computationally efficient and offers a good foundation for future studies. It can be used as a starting point, after which more advanced 2D models could be introduced to assess the performance of the HKN wind farm. By first developing a Jensen's 1D model and then comparing it with a new 2D model, results can be compared with real-time data. These findings can be used to draw conclusions on the effectiveness of wake models.

4.4 Comparison of Different Wake Models

As discussed in the previous section, extending Jensen's 1D wake model to 2D versions, such as the Jensen 2D and 2Dk models, offers a more realistic prediction of wake effects. The graph shown in Figure 4 shows that Jensen's 2Dk model produces results that are closest to those from Large Eddy Simulations (LES), further supporting the use of 2D extensions for improved wake prediction accuracy. However, it is worth noting that another comparison study by Gao et al. (2020) found that the Jensen-Gaussian model outperformed both Jensen's 1D and 2Dk models in certain scenarios.

The study by Gao et al. (2020) [37] compares Frandsen's 1D, Jensen's 1D and 2Dk, and the 2D Jensen-Gaussian model in three different scenarios; (a) one with a constant wind speed of 12 m/s and a fixed wind direction, (b) one with a constant wind speed of 12 m/s and variable wind directions, and (c) one with variable wind speeds of 8, 12, 17 m/s respectively and variable wind directions.

From their findings, it was concluded that for scenario (a), no major differences were found between the 1D and 2D models. In scenario (b), which involved changing wind directions, the two 2D wake models predicted the velocity profile more accurately than the 1D models. However, in scenario (c), the 2Dk model showed chaotic results. This behavior occurred because the velocity in the wake is described using a cosine function, which follows a repetitive cycle. Thus, while the Jensen 2Dk model offers accurate performance in somse cases, the Jensen-Gaussian model had the best performance results for the three scenarios [37].

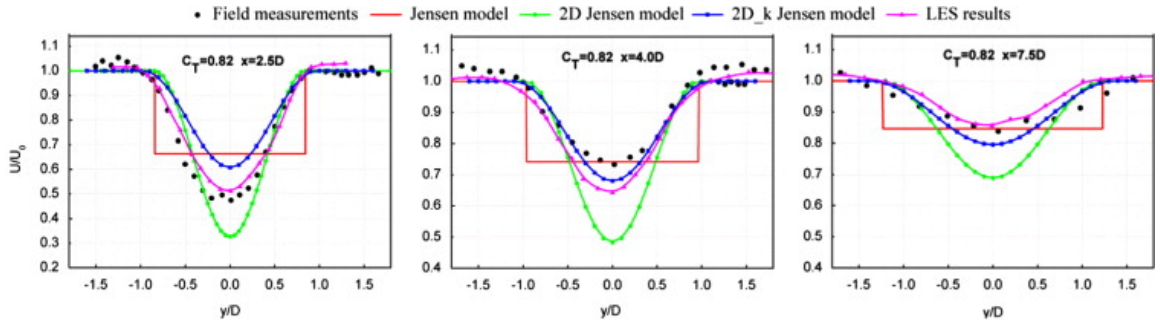

Figure 4: These graphs show the horizontal profile of the normalized velocity deficit at turbine hub height, plotted against the normalized axial distance, for various wake models. The comparison highlights the differences between Jensen's 1D, 2D, and 2Dk models. Notably, Jensen's 2Dk model produces results that most closely align with the LES (Large Eddy Simulation) results, demonstrating its improved accuracy in capturing wake dynamics [35]

4.5 Jensen's 1D Single Wake Model

Jensen's 1D wake model was selected to analyze wake effects, as explained in the previous section to offer a solid foundation for future studies. Jensen's 1D model still enables the calculation of

velocity deficits across the farm while balancing computational efficiency with practical accuracy. This model also enabled to visually represent the effect of expanding wakes on downstream turbines, which is essential for calculating multiple wake effects.

As mentioned earlier Jensen's 1D wake model assumes that the velocity profile expands linearly and is only a function of the distance x [m] downstream. The x-direction in this case is defined as the direction of the incoming wind flow [19, 33]. The radius in the wake expands linearly as:

$$R_w(x) = R + kx \tag{1}$$

where k [-] is known as the wake decay constant, for which a constant value of 0.4 is used for offshore wind farms [19, 33]. R [m] is the radius of the wind turbine and x [m] denotes the distance downstream of the turbine in line with the wind direction.

The wind velocity deficit of one wind turbine is calculated including the wake radius as follows:

$$v_{ji}(x) = v_0 \left(1 - \left(\frac{R}{R_w(x)}\right)^2 \left(1 - \sqrt{1 - c_T}\right)\right) \tag{2}$$

where v_0 is the uninfluenced incoming wind speed [m/s], C_T is the thrust coefficient [-], and $v_w(x)$ [m/s] is the wind speed in the wake at any distance x [m] along the wind direction investigated [38, 36, 20]. A visual representation of Jensen's 1D single wake model is shown in Figure 5 where the near wake and fake wake regions are shown and the expansion of a wake with a linear velocity profile [31].

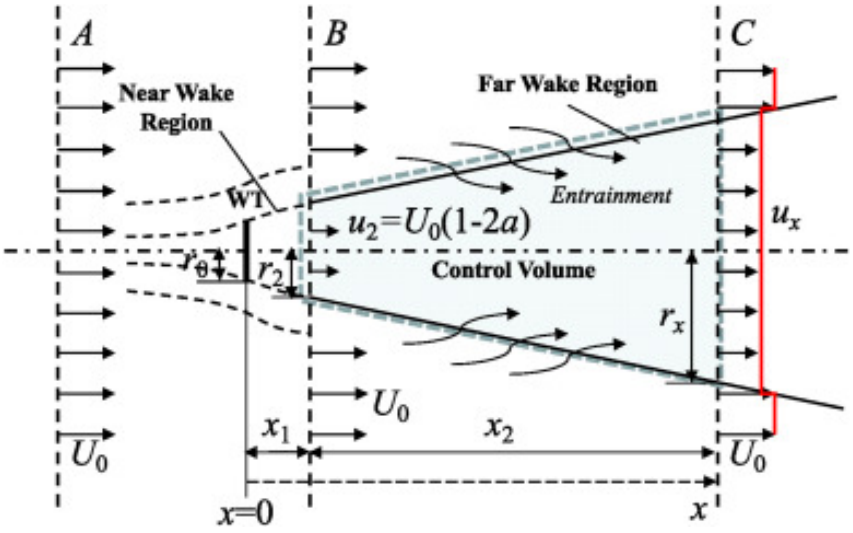

Figure 5: Jensen's single wake effect split up into three different regions, A, B, and C is shown in the figure. The wind speeds Ux [m/s] are identical along the vertical axis of each cross-section. Region A, which includes the area in front of the upstream turbine and the near wake region behind it, is characterized by significant wind speed reduction and increased turbulence due to energy extraction by the turbine rotor. In region B, the far wake, the wind velocity deficit recovers slowly and turbulence intensity decreases as the wake expands and mixes with the surrounding air. In region C, beyond the far wake region, the airflow has typically stabilized, and the velocity deficit and turbulence intensity are minimal, returning to ambient conditions [31].

4.6 Multiple Wake Model

Once the single wake effect has been calculated the next step is to calculate downstream overlapping wake effects, known as the multiple wake effect, by using one of the superposition

formulas. The four different superposition formulas are shown in Figure 6. Research by Shao et al. (2019) [18] provides that the precision and effect of the different superposition models on wind turbine's performance were tested and the model predictions were compared with wind tunnel experiments, leading to the Root Sum of Squares (RSS) model obtaining the most accurate results. Similarly, Tian et al (2017) [36] integrated the 2Dk Jensen Model into these four superposition models to calculate the power loss of a wind farm and compared the results to wind tunnel data leading to the same conclusion.

Using the RSS model together with the classical 1D Jensen model is actually the most commonly used method for predicting the wake deficit in wind farms, as shown in several studies [18]. The widely adopted use of the RSS model in combination with Jensen's 1D model, together with the established reliability of RSS led to the choice of using RSS for the multiple wake calculations in this research.

$$
\begin{aligned}
\textit{Geometric sum } (GS): &\quad \tfrac{u}{u_0} = \textstyle\prod_{j=1}^{n} \tfrac{u_j}{u_0} \\
\textit{Linear superposition } (LS): &\quad \left(1 - \tfrac{u}{u_0}\right) = \textstyle\sum_{j=1}^{n} \left(1 - \tfrac{u_j}{u_0}\right) \\
\textit{Energy of balance } (EOB): &\quad u_0^2 - u^2 = \textstyle\sum_{j=1}^{n} \left(u_0^2 - u_j^2\right) \\
\textit{Root sum of squares } (RSS): &\quad \left(1 - \tfrac{u}{u_0}\right)^2 = \textstyle\sum_{j=1}^{n} \left(1 - \tfrac{u_j}{u_0}\right)^2
\end{aligned}
$$

Figure 6: Four superposition Formulas for Calculating Multiple Wake Effects

Rewriting the RSS with the defined parameters in this research paper gives:

$$\left(1 - \frac{V_{wi}}{V_0}\right)^2 = \sum_{j}^{N_T} \left(1 - \frac{V_{ji}}{V_0}\right)^2 \tag{3}$$

where N_T is the total number of upstream turbines that affect the target turbine i and j denotes the specific downstream turbine that affects the target turbine i. v_{wi} [m/s] is the incoming velocity at target turbine i, v_0 [m/s] is the undisturbed initial velocity, and v_{ji} [m/s] denotes the wind speed at turbine i due to the single wake from turbine j. By rewriting the formula according to the steps presented below, the formula can be easily implemented into SIMSEN.

$$\frac{(V_0 - V_{wi})^2}{V_0^2} = \sum_{j}^{N_T} \frac{(V_0 - V_{ji})^2}{V_0^2} \tag{4}$$

$$(V_0 - V_{wi})^2 = \sum_{j}^{N_T} (V_0 - V_{ji})^2 \tag{5}$$

$$V_0 - V_{wi} = \sqrt{\sum_{j}^{N_T} (V_0 - V_{ji})^2} \tag{6}$$

$$V_{wi} = V_0 - \sqrt{\sum_{j}^{N_T} (V_0 - V_{ji})^2} \tag{7}$$

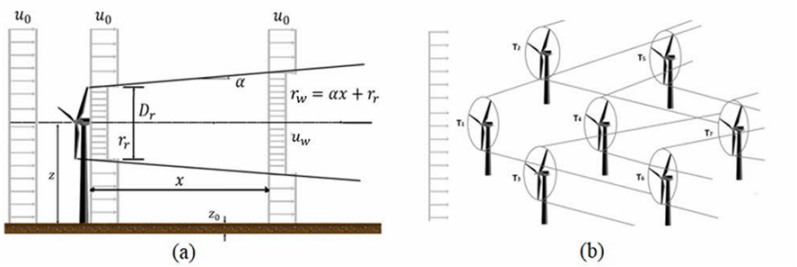

Figure 7: On the left, the 1D wake expansion behind a single wind turbine is illustrated according to Jensen's model. On the right, the overlapping of multiple wake effects is shown, representing how the wakes from multiple turbines interact and influence downstream turbines [39].

5 Mathematical Model

For accurately modeling the wind turbine's key parameters and its dynamics, it is essential to understand the underlying formulas. Section 5 introduces all the formulas and relationships that are necessary to model the wind turbine, excluding the effects of wake interactions and other surrounding influences.

As discussed in Section 4.1, the power output, power coefficient, tip speed ratio, blade pitch angle, and rotor speed were plotted as a function of wind velocity. These plots represent the general behavior of a single wind turbine in steady-state condition and all formulas attached to these different parameters will be introduced [40, 41].

To calculate the mechanical power that is produced by a wind turbine, it is considered that the kinetic energy E_v [J] in the air mass of an object m [kg], moving with a velocity v [m/s] is given by:

$$E_v = \frac{1}{2}mv^2. \tag{8}$$

Therefore, the power of moving air P_v [W], assuming that the wind speed C_∞ [m/s] is constant, P_v is determined by:

$$P_v = \frac{dE_v}{dx} = \frac{1}{2}\dot{m}C_\infty^2 \tag{9}$$

where $\dot{m}$ is the mass flow of air per second [kg/s]. As the air passes through an area A [m^2], considering the air density ρ [kg/m^3], the air mass flow is expressed by:

$$\dot{m} = \rho A C_\infty. \tag{10}$$

Applying Equation 10 in 9, the following is obtained:

$$P_v = \frac{1}{2}\rho A C_\infty^3. \tag{11}$$

Since A_{rot} is the rotor swept area of the turbine blades, it can be expressed by:

$$A_{rot} = \frac{\pi D_{rot}^2}{4} \tag{12}$$

where D_{rot} [m] is the rotor diameter.

The mechanical power transmitted by the fluid to the wind turbine can be expressed as:

$$P = \Delta p Q = \left(\frac{1}{2}\rho C_p C_\infty^2\right)(A_{rot} C_\infty) \tag{13}$$

where the pressure p [Pa], air density ρ [kg/m^3], power coefficient C_p, wind speed C_∞ [m/s], and the wind turbine cross section A_{ref} [m^2] are the key variables [40, 41].

This yields to:

$$P = \frac{1}{2}\rho A_{rot} C_p C_\infty^3. \tag{14}$$

The power coefficient C_p [-] represents how efficiently a wind turbine converts the energy in the wind into mechanical power. It shows the proportion of the wind's energy that is captured by the rotor blades and is a function of the TSR λ [-] and the blade pitch angle θ [deg] [42]:

$$C_p = C_p(\lambda, \theta).$$

The blade pitch angle is based on a lookup table in this research and the TSR λ [-] is given by:

$$\lambda = \frac{D_{rot}\omega}{2C_\infty} \tag{15}$$

where ω is the rotor speed expressed in [rad/s] and is given by: [41]

$$\omega = \frac{\lambda 2C_\infty}{D_{rot}}. \tag{16}$$

The TSR is set to its constant optimal value in region II, as explained in Section 4.1, to maximize power extraction. As D_{rot} [m] is constant, the rotor speed ω [rad/s] should increase proportionally to the wind speed C_{inf}. This is only possible in the operating range of a wind turbine, which is bounded by $\omega_{\min}$ and $\omega_{\max}$. To use a simple approach that includes this information, the rotor speed is modeled based on the following [27]:

$$\omega = \min\left(\omega_{\max}, \max\left(\omega_{\min}, \frac{\lambda_{\text{opt}} C_\infty}{\frac{D_{\text{rot}}}{2}}\right)\right). \tag{17}$$

The aerodynamic torque T [Nm] that is generated as the wind exerts force on the blades, causing them to rotate around the turbine's hub, is calculated by the following formula:

$$T = \frac{P}{\omega}. \tag{18}$$

Saint et al. (2020) provides a generic approximation for the power coefficient based on six different exponential models, which can be found in Appendix Table 8. The values that have been used for the parameters in the research by Saint et al. (2020) [27] are presented in 1. These values will also be used for this model to be able to compare and validate the model based on the model by Saint et al. (2020) [27]:

$$C_p(\lambda, \theta) = c_1\left(\frac{c_2}{\lambda_i} - c_3\theta - c_4\lambda_i\theta - c_5\theta^z - c_6\right)\exp\left(-\frac{c_7}{\lambda_i}\right) + c_8\lambda \tag{19}$$

where

$$\lambda_i = \frac{1}{\frac{1}{\lambda + c_9\theta} - \frac{1}{c_{10}(\theta^3+1)}}. \tag{20}$$

Table 1: Parameter values for the Cp formula

Parameter	c_1	c_2	c_3	c_4	c_5	c_6	c_7	c_8	c_9	c_{10}	z
Value	0.22	120	0.4	0	0	5	12.5	0	0.08	0.035	0

The maximum aerodynamic efficiency of the power coefficient, known as the Betz limit, is $C_{p,opt} = 0.59259$, representing the theoretical maximum fraction of power that can be extracted from an ideal wind stream. The power coefficient and the thrust coefficient are related through axial induction factor a [-]. The axial induction factor represents the factional decrease in wind speed between free stream and rotor plane, where $a = 0$ indicates that none of the winds energy is extracted by the turbine and $a = 1$ indicates that the turbine extracts all the wind's kinetic energy [43, 44, 45, 46].

For most practical wind turbine designs the factor usually does not exceed 0.6. In well-optimized turbine blades a tends to be around 0.33 during most of the turbine's operational range, which

aligns with Betz limit for efficient power extraction. Considering that $0 < a < 1$ and a rarely exceeds 0.6 the values of a can be obtained by solving $C_P = 4a(1-a)^2$ [45]. The thrust coefficient C_T is used for the wake effect calculations, which represents the ratio of the axial thrust force Fa [N] on the turbine blades to the dynamic pressure of the incoming wind. The C_T [-] is related to Cp [-] as shown in Equation 24 and will be defined based on the power coefficient curve of the SIMSEN model:

$$C_P = 4a(1-a)^2. \tag{21}$$

Rewriting Equation 21 for obtaining the axial induction factor gives:

$$C_P = 4a^3 - 8a^2 + 4a. \tag{22}$$

Solving Equation 23 for a [-] will result in three different solutions.

$$4a^3 - 8a^2 + 4a - C_P = 0, \tag{23}$$

$$a1, a2, \text{and } a3.$$

These values are shown in Appendix Table 9. With the obtained values for a, the thrust coefficient can be determined based on the following equation:

$$C_T = 4a(1-a). \tag{24}$$

The axial thrust could then be calculated using the following expression [45, 47]:

$$F_a = \frac{1}{2}\rho A_{\text{rot}} C_T C_\infty^2. \tag{25}$$

These equations will be used for a case-study on HKN, where real-life data will be used for the input parameters of the models.

6 Simulation Setup SIMSEN

This section further explains how SIMSEN is used for modeling a wind farm, with the specific simulation parameters and building blocks.

6.1 Building Blocks SIMSEN

For building a model based on the mathematical formulas described in Section 5 and lookup data, different functions have been used in SIMSEN. For the lookup data a points function is implemented in SIMSEN. This function allows to introduce special curves that could be difficult to introduce with the program unit. The input signal x of this unit is equal to the sum of all the inputs xi (REFERENCES X). The Points Function provides one output signal y. The data points are specified in a table where each point has an x value and a corresponding y value. This is similar to a lookup table. The only difference is that a lookup table provides direct input-to-output mapping, while the SIMSEN Points Function offers advanced features such as summing inputs, smoothing, and handling complex relationships.

A program unit is used for the calculation of all parameters that are defined by a formula, such as the TSR [-], ω_{rot} [rad/s], the Cp [-] and the C_T. The user can calculate diverse logical and mathematical functions with only one block. It uses the input values xi (REFERENCES X) and generates up to 20 output values yi that can be read from another unit, where i represents a counting number (1,2,3,4,...,100). In the DATA section constant values can be added, such as a blade radius of R=100 [m] for example.

The wind turbine built-in block (see Figure 8) calculates the power output and the torque based on the formulas in section 5. However, for the calculation of the axial thrust Fa [N] the power coefficient is used instead of the thrust coefficient which does not fully accurately represent the thrust force as Cp and C_T are related through axial induction factor a but do not represent the same The wind turbine built-in block (see Figure 8) is designed to calculate power output and torque based on the formulas detailed in Section 5. However, for determining the axial thrust Fa [N], the power coefficient Cp [-] is used instead of the thrust coefficient C_T. This approach introduces inaccuracies, as Cp and C_T represent different physical behaviors as introduced in Section 5. Cp focuses on power extraction efficiency, while C_T represents the aerodynamic thrust force acting on the rotor. As a result, this substitution may lead to an incomplete representation of the actual thrust force exerted on the wind turbine.

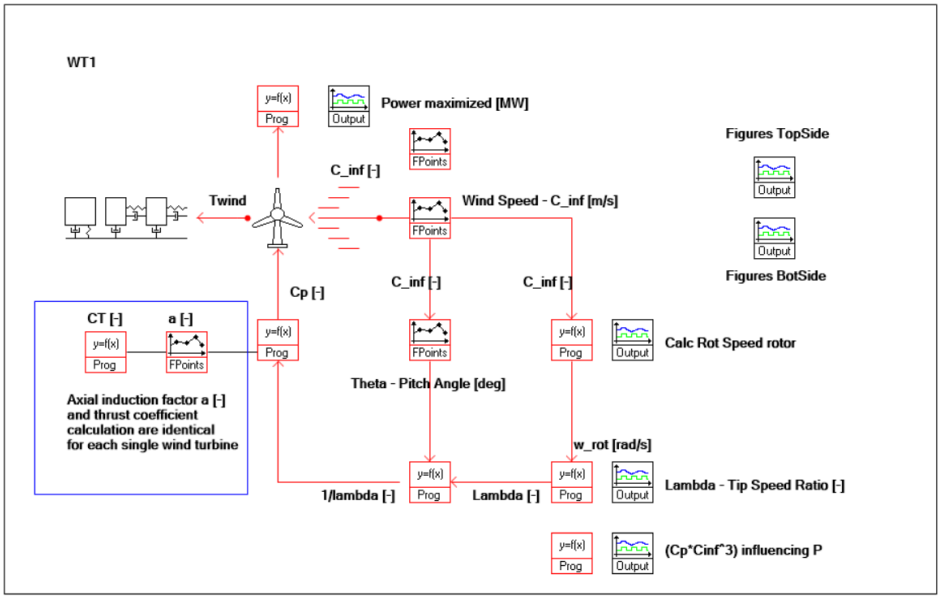

Figure 8: SIMSEN Model of a Single 11 MW Wind Turbine

6.2 Sensitivity Analysis 24h One Wind Turbine

A sensitivity analysis has been performed for the single wind turbine SIMSEN model as this model serves as the base model for each wind turbine throughout the wind farm. From the results shown in Table 2 it can be observed that from an integration time step of 0.01 seconds, the extracted data is no longer influenced. It is therefore decided that an integration time step of 0.01 seconds will be used for the simulations as this is more time convenient than smaller time steps while still giving the same results.

Table 2: Sensitivity Analysis Results for Different Integration Time Steps.

Integration Time Step [s]	**Average Power Output per Hour [MW]**	**Maximum Power Output [MW]**	**Energy Yield over 24h [MWh]**
0.0001	7.4615	11	186.54
0.001	7.4615	11	186.54
0.01	7.4615	11	186.54
0.1	7.4562	11	186.41

6.3 Simulation Parameters

The simulation parameters that need to be defined when running a model are displayed in Table 3, with the corresponding units and values used for the modeling of single and multiple wind turbines. A lookup table was used to simulate over 24 hours while the maximum duration was still 125 seconds. This allowed to quickly obtain results.

Table 3: Simulation Parameters

Parameter	**Unit**	**Value**	**Description**
Time min	sec	0.0000E+000	Start time of the simulation.
Time max	sec	1.2500E+002	Maximum duration of the simulation (125 seconds).
Integration step	sec	1.0000E-002	Time interval for the numerical solver (0.01 seconds).
Precision for immediate events	%	1.0000E+000	Precision for handling immediate events during the simulation.
Precision for simultaneous events	%	1.0000E+000	Precision for managing simultaneous events during the simulation.
Integration process	-	RK45	Numerical integration method used (Runge-Kutta 45).
Write in output files every	-	1.0000E+001	Frequency of writing simulation outputs (every 10 steps).
Initial conditions from	E/M/C	E	E = Element, M = Main File and C = Combined. If E is selected, the program sets initial value of all the state variables to the corresponding value defined in each element' own INTIAL CONDITIONS section.
Disturbances activated	Y/N	NO	Indicates whether disturbances are activated during the simulation.

6.4 From One Wind Turbine To a Wind Farm

Once the single wind turbine was validated, its code was duplicated for additional turbines. The turbines were positioned and numbered in the model to match their layout in GeoGebra [48], allowing easy identification of turbines affected by wake effects from upstream ones. Turbines that were most upstream in the layout (e.g., WT1) used the same wind velocity input. For downstream turbines affected by wake effects, modifications were made to include all individual wake disturbances. This was achieved by adding program blocks to account for each wake effect impacting the target turbine.

7 Hollandse Kust Noord Case Setup

This section provides all necessary data that needs to be defined in order to accurately model HKN in SIMSEN, followed by the different case setups will be explained.

7.1 Hollandse Kust Noord

The system modeled and analyzed in this BaIP begins with a single wind turbine in SIMSEN. This wind turbine must operate similarly to the defined operational regions explained in 4.1 to ensure that the model performs as specified. After validating the single wind turbine model, it will be expanded to represent the HKN (HKN) wind farm in the North Sea. Instead of applying equivalent conditions as done by Nicolet et al. (2014) [12], the individual performance of each turbine is considered. This site was chosen because it is one of the Netherlands' largest operational wind farms, with a total capacity of 759 MW [49].

HKN consists of 69 Siemens SG 11.0-200 DD offshore wind turbines. Each turbine has a hub height of 125.5 meters, a rotor diameter of 200 meters, blade lengths of 97 meters and a swept area of around 31416 m2. The nominal power output of each turbine equals 11 MW by which the total output of 759 MW is realized. These turbines are distributed over an effective area of 92 km2 where most of them are placed more than one kilometer apart from one another [50]. The Siemens Gamesa SG 11.0-200 DD wind turbines have a cut-in wind speed of 4.0 m/s, a rated wind speed of 14 m/s and a cut-out wind speed of 32 m/s. These values will be used to investigate the different regions for the 11MW wind turbine. [51]

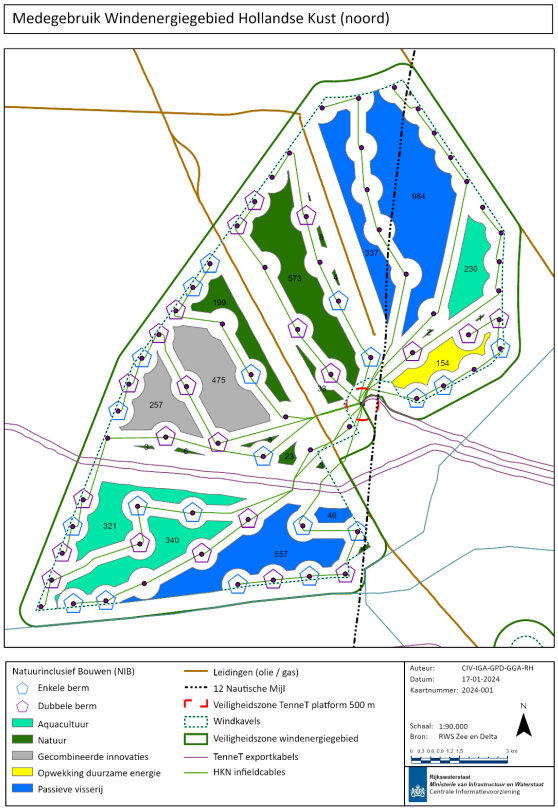

Figure 9: Locations of all wind turbines at HKN with scale [49]

7.2 Hollandse Kust Noord Case Scenarios

To analyze wake effects at HKN, two case studies were conducted using wind data. These case studies aim to provide insights about the influence of wind pattern fluctuations on the performance and layout of the wind farm HKN. The first case study evaluates the impact of a 270° Western wind direction on the energy yield, while the second evaluates a 225° Southwestern wind direction to account for the two most dominant wind patterns at the site.

Wind data for these case studies was obtained from Windfinder [23], which provides hourly wind speeds and directions over a 24-hour period as shown in Appendix Table 5. The average wind direction obtained from a regular day in December 2024 was 267° West, which was rounded to 270° West for simplicity. Additionally, the wind rose in Figure 10 illustrates wind patterns from 1999 to 2013 at 128 meters altitude, corresponding to the hub height of 125.5 meters at HKN. It specifically shows that SSW and WSW are the most common wind directions at HKN. Since the hub heights of the wind turbines at HKN are approximately 125.5 meters, this wind rose was considered the most representative.

The 270° West direction was selected for the first case study, as it was both the average of the 24-hour dataset and the third most frequent direction according to the wind rose. The second case study evaluates the 225° Southwest direction, representing the average of the two dominant wind directions (SSW and WSW). Both case studies use the same hourly wind speeds obtained from Windfinder to clearly observe the impact of different wind directions on wake effects [52].

Since the layout is fixed in HKN, the evaluation would also focus on how well the turbines are distributed to minimize wake effects. As the prediction accuracy of wake models is highly affected by the spacing and downstream distance between wind turbines, it is important to use the precise locations at the chosen site. Due to the absence of precise coordinates for the turbines at HKN, a scaled map (Figure 9) was used to obtain the positions of the turbines as accurate as possible. These positions were implemented in GeoGebra [48], a measurement tool, to analyze and extract precise values from the geometric construction of the wind farm. With the use of GeoGebra the exact inter-turbine distances could be easily calculated based on the newly created scale. This is further explained in 8.8.

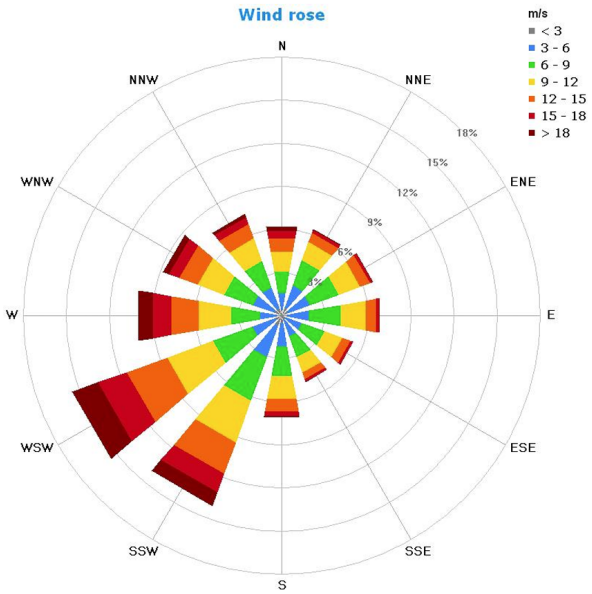

Figure 10: Hollande Kust Noord Wind Rose at 128m High from 1999-2013 [52]

To optimize the analysis process and focus on delivering results within the given time frame, the lower 19 turbines of HKN are initially modeled. This selection provides a representative segment of the wind farm that allows for a manageable starting point to test the methodology and validate the approach, particularly the wake effect calculations and RSS. In figure 11 the wake effects are shown resulting from a 270 degrees Western wind flow.

In Figure 12 the wake effects caused by setting the wind direction constant at 225 degrees South West are shown. Comparing this Figure with Figure 11, it can be immediately observed that less downstream wind turbines are affected by the wakes of upstream turbines than in Case I. This is therefore also expected to be the outcome of these two cases in terms of velocity deficits and power outputs. The distances between all downstream turbines affected by an upstream turbine are shown in Appendix Table 6 for Case I and 7 for Case II.

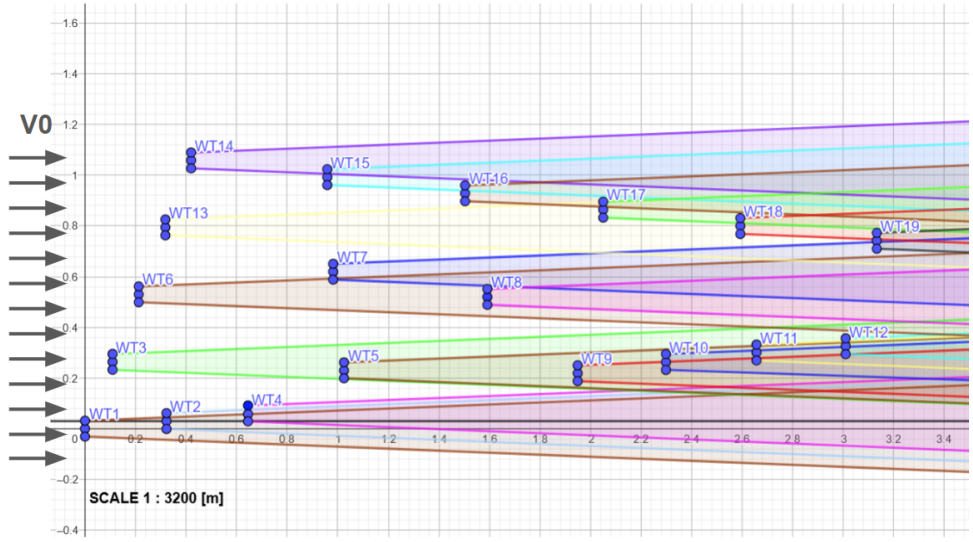

Figure 11: Wind Turbines with Wake Effects Plotted Based on Jensen's 1D Wake Model for a 270° West Wind Direction

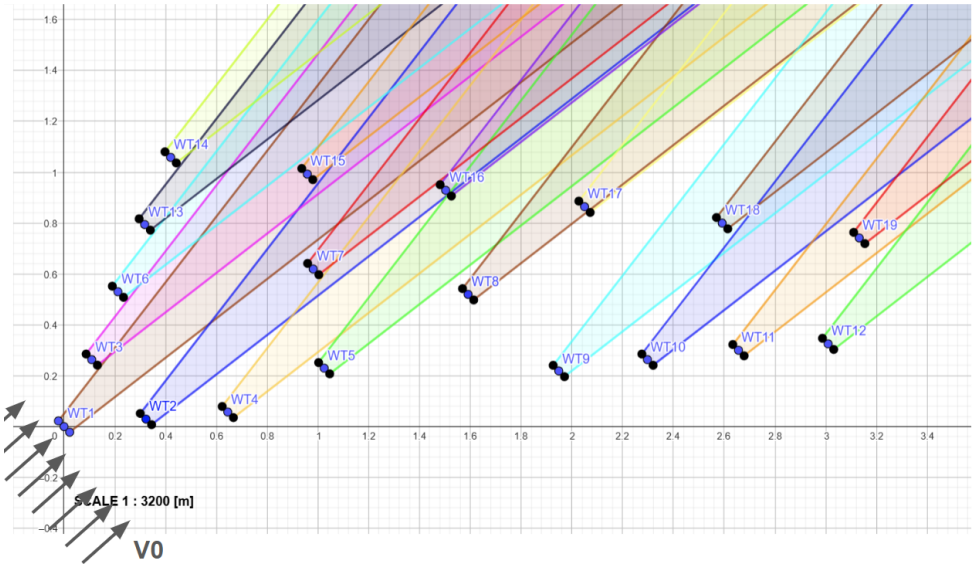

Figure 12: Wind Turbines with Wake Effects Plotted Based on Jensen's 1D Wake Model for a 225° Southwest Wind Direction

8 Assumptions and Key Considerations for Modeling HKN in SIMSEN

This section outlines and elaborates on the key assumptions and considerations made in modeling the wake effects of the HKN wind farm.

8.1 Identical Behavior of Each Single Turbine

It is important to understand that all the wind turbines at the HKN site are identical, indicating that the turbines will exhibit similar behavior at corresponding wind speeds. Consequently, parameters such as the minimum and maximum rotational speeds, the optimal tip speed ratio, the pitch angle lookup table, and, by extension, the power coefficient at different wind speeds, are all considered constant across turbines.

However, when modeling an entire wind farm, rather than a single turbine, variations in velocity deficits due to wake effects must be accounted for. A downstream turbine is assumed to behave identically to the upstream turbine that is not influenced by the wake as explained previously. The primary distinction is that the downstream turbine experiences a delay in reaching the wind speed characteristic of the upstream turbine, causing its power curve to lag behind. This delay results in a both a spatial- and time-dependent difference in performance between turbines, which are critical factors in accurately simulating the behavior of wind farms as a whole.

8.2 Determination of Optimal Tip Speed Ratio

The optimal TSR [-] was determined through an iterative process. By systematically adjusting the TSR and evaluating the corresponding power coefficient at each step, the value that maximized Cp was identified. In region II, the objective of the optimal TSR is to maximize the power output by keeping the power coefficient constant at its maximum value for increasing wind speeds. Through this process, an optimal TSR of 6.5 [-] was obtained, giving a maximized Cp of 0.425 [-]. This value not only ensures the highest aerodynamic efficiency but also smoothens the Cp-curve, by which any irregularities or inaccuracies are avoided. The TSR of 6.5 will be used as a key parameter for modeling the wind turbine's behavior.

8.3 Pitch Angle Lookup Table

For the pitch angle, a lookup table was initially created based on the curve presented in the research by Saint et al. (2020) [27]. This curve was used for modeling the 2 MW turbine. Since no exact values are provided in the research paper, the newly created curve will not be completely identical to the one shown in the research by Saint et al. (2020). As the pitch angle directly influences the power coefficient's behavior, the Cp curve will also not match exactly to the one presented in the article.

Previous studies by Saint et al. (2020), Liew et al. (2020), and the IEA Wind TCP Task 37 technical report (2019) [27, 53, 54] did not show significant differences between the pitch regulation of a 2 MW turbine and a 10 MW turbine, as illustrated in Figure 13. Therefore, it is expected that the pitch behavior of the 11 MW turbine will also be comparable to that of the 2 MW and 10 MW turbines.

Although the curves are very similar, they are not completely identical and therefore the pitch angle curve of the 10 MW turbine was chosen for modeling the 11 MW turbine. This is due to the fact that a 10 MW turbine lies more in the range to an 11 MW turbine than a 2 MW turbine and because of the direct lookup table that is provided by the IEA Wind TCP Task 37 technical report (2019) [54].

Nonetheless, it is important to note that this lookup table was based on a rated wind speed of 11 m/s, whereas the 11 MW turbine has a rated wind speed of 14 m/s [55]. To address this, the values in the lookup table were shifted to align with the 14 m/s rated wind speed as part of the blade pitch control strategy. Additionally, the values were adjusted in such a way that the pitch angle stays zero between cut-in and rated wind speed, as this was also explained in Section 4.1. This newly created lookup table can be found in Appendix Table 10.

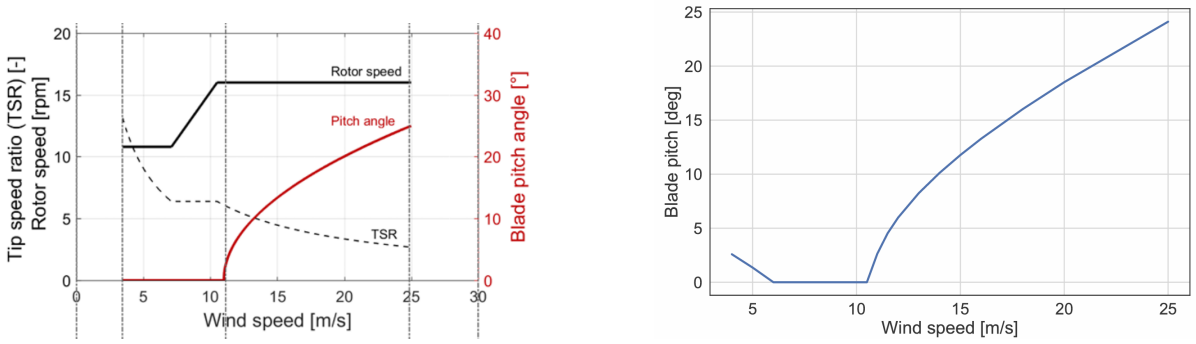

(a) *(b)*

Figure 13: Pitch Angle Curve of (a) a 2 MW turbine where the pitch angle is adjusted for a rated wind speed of 11 m/s to regulate power output [27], and (b) a 10 MW turbine where the pitch angle is adjusted to a rated wind speed of 10.75 m/s to regulate power output [54]

8.4 Determination wmin and wmax

In the paper by Saint et al. (2020) [27], formulas for calculating the minimum and maximum rotor speed are presented. However, implementing the formula for these rotor speed limits in the 2 MW base model gives different outcomes than the minimum and maximum rotor speed that are presented in their graph. The graph of a 2 MW turbine in the research by Saint et al. (2020) [27] provides a minium rotor speed of around 10.8 RPM and a maximum rotor speed of around 16 RPM for a $D_{rotor} = 80m$, while the formulas in their article give the following estimation of the rotor speed being:

$$wmin = 1046.558 D_{rotor}^{-1.0911} = 8.776\,\text{RPM}$$
$$wmax = 705.406 D_{rotor}^{-0.8349} = 18.178\,\text{RPM}$$

It is assumed that the values in their graph were obtained by previous works. Therefore, to match the 2 MW SIMSEN model for validation, the minimum and maximum rotor speed have been extracted from the graph instead of using the formulas. When adjusting the model to a 11 MW turbine, different sources have been used to ensure that the scaling of the system behaves within in the desired operating range of the turbine. The minimum and maximum values for 10 MW wind turbines could be found in literature. As a 10 MW turbine is considered to lie within an acceptable range compared to the 11 MW turbine, the average of five different sources has been used. First of all, the general formulas provided by Saint et al. (2020) [27] were used to estimate the rotor speed limits for a $D_{rotor} = 200m$:

$$wmin = 1046.558 D_{rotor}^{-1.0911} = 3.229\,\text{RPM}$$
$$wmax = 705.406 D_{rotor}^{-0.8349} = 8.459\,\text{RPM}$$

A $wmin = 0.62$ rad/s $= 5.921$ RPM and a $wmax = 0.905$ rad/s $= 8.642$ RPM were obtained from Liew et al. (2020) for the IEA 10 MW turbine [53]. All of the maximum and minimum

rotor speeds are displayed in 4, from which an average $wmin = 5.288$ RPM and a $wmax = 8.896$ RPM were obtained. These values will be used for modeling the 11 MW turbine.

Table 4: Overview of ω_{min} and ω_{max} values from different sources.

Turbine Type and Source	ω_{min} **(RPM)**	ω_{max} **(RPM)**
10 MW IEA Turbine [53]	5.921	8.642
10 MW DTU Turbine [56]	6.0	9.6
10 MW Turbine [54]	6.0	8.68
11 MW SG Turbine [55]	–	9.1
Any Turbine [27]	3.229	8.459
Average	**5.288**	**8.896**

8.5 Thrust Coefficient

The thrust coefficient C_T [-] is a dimensionless value that represents the ratio of the actual aerodynamic thrust force on the wind turbine blades to the dynamic force in the wind that is available for extraction. To determine the thrust coefficient no direct values could be obtained from the SIMSEN model. This is due to the fact that in the built-in SISMEN wind turbine block, the axial thrust is calculated based on the Cp which can't be changed [40]. Thus, when trying to extract the C_T values in steady-state from the thrust graph, this will result in the values of Cp [-].

Based on Equation 21 and 24 the C_T could be manually calculated. By solving Equation 23 with Cp values extracted from the Cp curve in SIMSEN shown in Figure 14, the axial induction factor a [-] could be calculated.

Based on the domains defined in Section 5, where $0 < a < 1$ and a rarely exceeds 0.6, one of the three solutions obtained by solving Equation 23 immediately cancels out as it exceeds the upper limit of 1. For the remaining two solutions, this research defines $a < 0.6$ as the valid range. Appendix Table 9 presents the three solutions for each Cp value that result from solving Equation 23. Among the solutions, only the values for a_1 satisfied the condition $a < 0.6$ for all Cp values. Therefore, these axial induction factors were used for calculating the C_T.

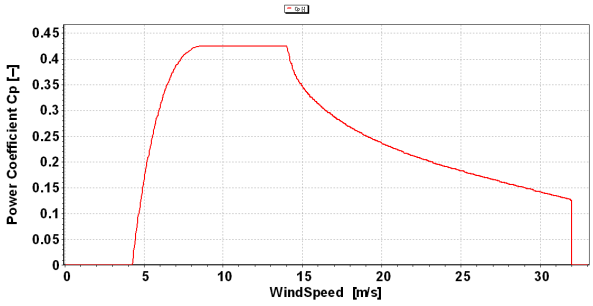

Figure 14: Cp Curve of the 11 MW Wind Turbine

8.6 Limit on Power Output

Wind turbines are designed to keep the power output constant at its rated value for wind speeds exceeding the rated wind speed [27]. A constraint has been added in the SIMSEN model that maximizes the power output to 11MW once the power curve exceeds this value, which is the rated power output of the wind turbine. Since generator torque control is not explicitly implemented in the current SIMSEN model, the power output constraint serves more as a protective measure

rather than a direct control over the torque. This added constraint of the model helps prevent unrealistic power generation at higher wind speeds than rated wind speeds.

8.7 Time Delays

When analyzing Jensen's 1D wake model an important observation is that this model primarily focuses on the spatial effects of the wake, where the wake deficit in wind speed is a function of the distance downstream from the turbine. However, the model doesn't explicitly account for time delays. Thus the results that are obtained in this research only provide insights on the effect of the spatial distance between turbines on their velocity deficits and thereby power outputs. As it takes time to travel downstream to the other turbine this is highly important for accurately evaluating the performance of a wind farm and is suggested to include for future studies.

8.8 Scale of Hollandse Kust Noord

Due to the unavailability of exact coordinates for the wind turbines located at the HKN offshore wind farm, an alternative approach was necessary to create an accurate representation of the turbine layout as explained in 7.1. To overcome this limitation, GeoGebra was used to construct a new scale model [48].

The first step involved plotting the dots from the provided Figure (9), placing them precisely at the same positions as indicated in the original image. Using the given scale in the Figure, the real distances between Wind Turbine 1 (WT1) and Wind Turbine 2 (WT2), as well as between WT1 and Wind Turbine 3 (WT3) were calculated. These distances served as the foundation for establishing the scale of the plot.

With the real-world distances determined, the scale of the newly created plot was calculated based on the measurements between specific wind turbines. The real-life distance between WT1 and WT2 was 1.02 km, while the corresponding distance in the plot was 0.32 units. This resulted in a scale calculation of 0.32:1.02 km, which simplifies to 0.32:1020 m, yielding a scale of 1:3187.5 m.

Similarly, the real-life distance between WT1 and WT3 was 0.9 km, with the plot distance being 0.28 units. This gave a scale calculation of 0.28:0.9 km, which simplifies to 0.28:900 m, resulting in a scale of 1:3214 m.

To ensure consistency and accuracy, the average of these two scales was taken:

$$\text{Average scale} = \frac{3187.5 + 3214}{2} \approx 3200\,\text{m}$$

Thus, a final scale of 1:3200 m was established for the entire wind farm layout. This approach ensured a reliable and consistent representation of the turbine positions in the plot. With this new scale all distances could be determined between the different turbines of HKN for the wake effect calculations.

8.9 Single Wake Effects

For the single wake effects, the wind speed at the upstream turbine is considered the initial wind speed. For the downstream turbine, the distance x in the wind direction represents the precise distance between the center of the upstream turbine and the center of the downstream turbine. Using perpendicular lines in GeoGebra this distance can be calculated exactly. Two examples (one for each wind direction) of how these distances were obtained are shown in Figure 15.

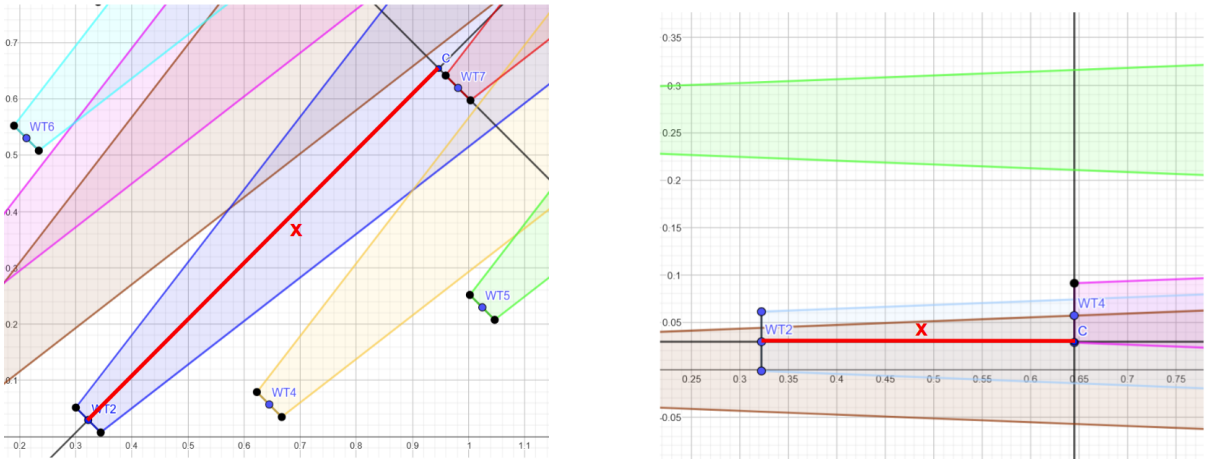

(a) *(b)*

Figure 15: Example of Computed Distance (a) Between Turbine 2 and 7 for 225 Degrees SouthWestern Wind Speeds, and (b) Between Turbine 2 and 4 for 270 degrees Western Wind Speeds

A disadvantage of Jensen's original 1D wake model is that no partial wake theorem is included. Thus if only one part of a turbine's rotor plane is affected by the wake of the upstream turbine, the wake velocity deficit will be over-predicted when Jensen's original model is implemented. An example of a wake in which velocity deficit will be highly over predicted is shown in 16. This wake effect occurring in Case I is considered negligibly small as only a very small part of WT7's rotor place is affected by the wake of WT6. For all other wake effects in both case I and II no partial wake effects have been taken into account. For future research, accounting for partial wake effects is highly recommended as this significantly influences the expected velocity deficits [36].

Currently in both SIMSEN models no partial wake effects were considered. The only wake effect that was considered negligibly small is the influence of WT6 on WT7 in the 270 degrees West Model. In 16 this partial wake is shown. However it is highly important to account for partial wakes for all downstream turbines as this is part of indicating the influence on velocity deficits [36]. Research by Tian et al. (2017) [36] states that Jensen's $2D_k$ model doesn't need additional partial wake corrections since the model already has a two-dimensional feature. Therefore the current model could be extended easily to Jensen's $2D_k$ model as only a few adjustments have to be made in the already implemented formulas.

Another paper investigates the influence of full and partial wakes on the power output of wind turbines within a wind farm based on Jensen's 1D model. This paper could also be used to further explore how to effectively account for partial wake effects within a wind farm [57].

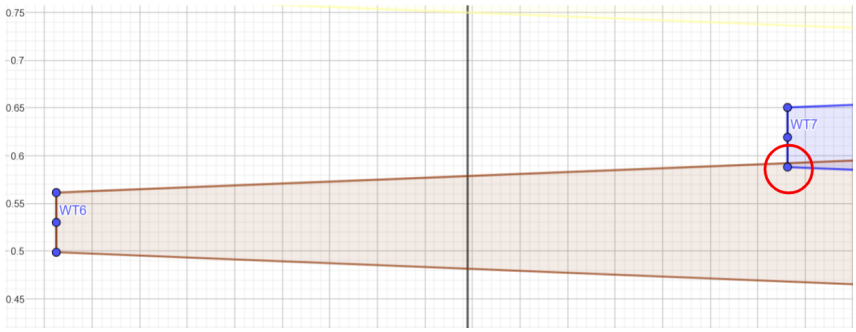

Figure 16: Partial Wake Effect of WT6 on WT7 Assumed Negligibly Small.

8.10 Multiple Wake Effects

As discussed in Section 8.9, the wake effects from upstream turbines on downstream turbines are modeled assuming full wake impact, except for the wake effect of WT6 on WT7. In the current model, the wake from each upstream turbine is considered for all downstream turbines where the wake intersects the rotor diameter. For the multiple wake calculations, it is assumed that each wake persists for at least 64 rotor diameters downstream. This assumption is based on the findings of Dong et al. (2022) [58], who reported that wind velocity in a wind farm wake recovers 95 percent after 55 rotor diameters downstream.

The choice of 64 rotor diameters ensures that the model captures the full extent of wake effects on all 19 investigated downstream turbines in the wind farm. This slightly overestimated approach minimizes the risk of overlooking significant wake interactions. For modeling the multiple wake effect, each upstream turbine's single wake effect on the target turbine is first calculated and afterwards all these results are combined by the tip speed formula.

9 Model Results

This section provided the results of the models that were created in SIMSEN. First, the validation of the single wind turbine models are discussed. Afterwards, the results obtained by the two case scenarios are discussed.

9.1 2 MW Single Wind Turbine

The first step to be made was recreating a 2MW wind turbine model based on the article written by Saint et al. (2020) [27]. The curves obtained by the SIMSEN model are shown in 17 and completely correspond to the curves obtained by Saint et al. (2020). The only differences, as explained in 8.3, are that the pitch angle, and Cp curve are slightly different. This is due to the approximated values of the pitch angle that were extracted from the graph by Saint et al.(2020). As this small inconsistency is for now assumed to be negligible the 2 MW model is validated. [59]

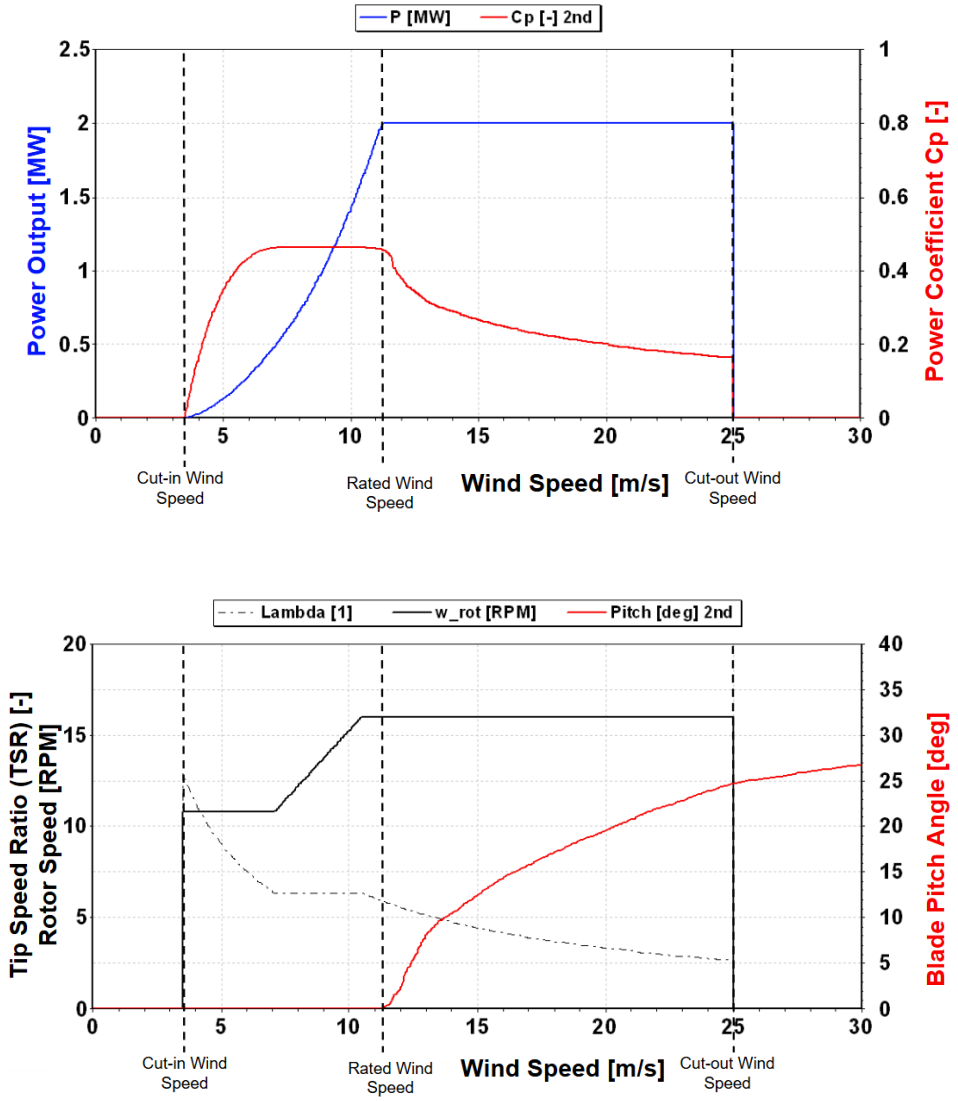

Figure 17: 2 MW Turbine With Its Different Operational Regions and the Corresponding Cut-in, Rated, and Cut-out Wind Speeds

9.2 11 MW Single Wind Turbine

Once the 2 MW wind turbine model was validated, its parameters were adjusted to match the 11 MW turbines placed at HKN. The 11 MW turbine behavior with the adjusted cut-in, rated, and cut-out wind speeds obtained by [55] is shown in 18. It can be observed that the power curve does not correspond to a rated wind speed of 14 m/s but instead to a speed of 11 m/s.As observed in other research such as the one by Saint et al. (2020), [53], and the IEA Wind TCP Task 37 technical report (2019) [27, 54], the power outputs do reach their rated power once the rated wind speed is reached. Therefore, there might be an inconsistency in the newly created model.

After carefully examining the model and its associated formulas, it can be concluded that the power curve below the rated wind speed primarily depends on the increasing wind speed C_∞, the power coefficient Cp [-], λ_i, the TSR [-], and w_{rot} [rad/s]. The pitch angle θ [deg] is not explicitly a factor in this region, as the angle is set to zero below rated wind speed according to the control strategy defined in Section 4.1.

Since the Cp [-] and λ_i are approximated formulas based on scientific research, where different values can be chosen, one solution would be checking whether changing these values (outlined in Table 8 in the Appendix) with their corresponding optimal TSR [-] would solve the issue. However, none of the alternative values tested resulted in a power curve behaving towards a rated wind speed of 14 m/s. Then, it was checked whether calibrating the TSR [-] within the model would work. Unfortunately, it was observed that changes in TSR only produced a minor decrease in the power curve. This also led to irregularities in the Cp curve and was insufficient to address the discrepancy of the power curve.

w_{rot} [rad/s] is constrained by an upper and lower limit, which can't be changed without justification for this purpose. Given that these parameters are the primary factors influencing the power curve, and further adjustments failed to achieve the desired results, it was ultimately decided to leave the model as is. This might lead to over predicted performance of the wind farm.

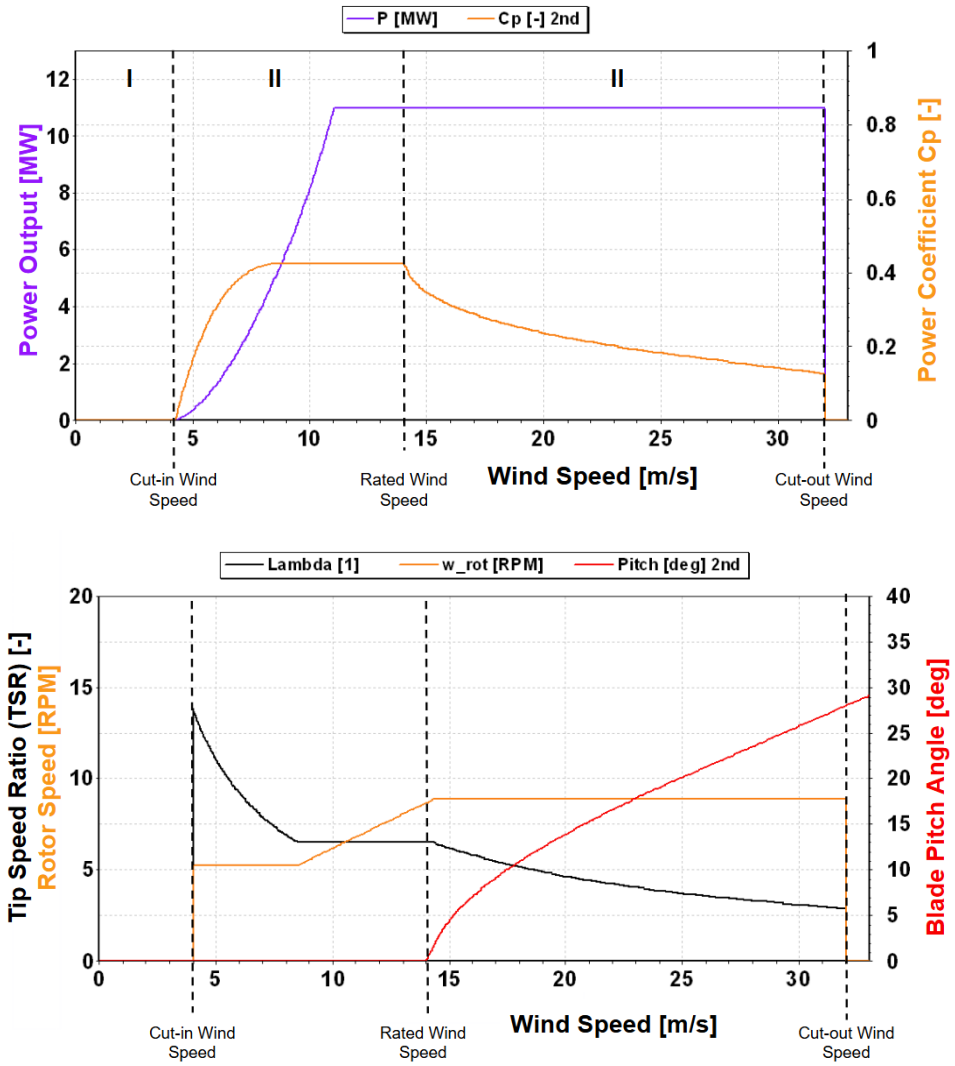

Figure 18: 11 MW Turbine With Its Different Operational Regions in Steady-State and a Cut-in, Rated, and Cut-out Wind Speed of 4, 14, 32 m/s Respectively

9.3 Effect of Fluctuating Wind Speeds

Fluctuating wind speeds significantly impact the power output of wind turbines, as wind speeds constantly vary in real life. This section illustrates how these fluctuations affect turbine performance. Figure 19 compares the power output of a single turbine under linearly increasing wind speeds to that under fluctuating wind speeds. The intention of these figures is to only highlight the impact of fluctuating wind speeds on turbine performance. However, it is important to note that linearly increasing wind speeds are not realistic in real-life scenarios.

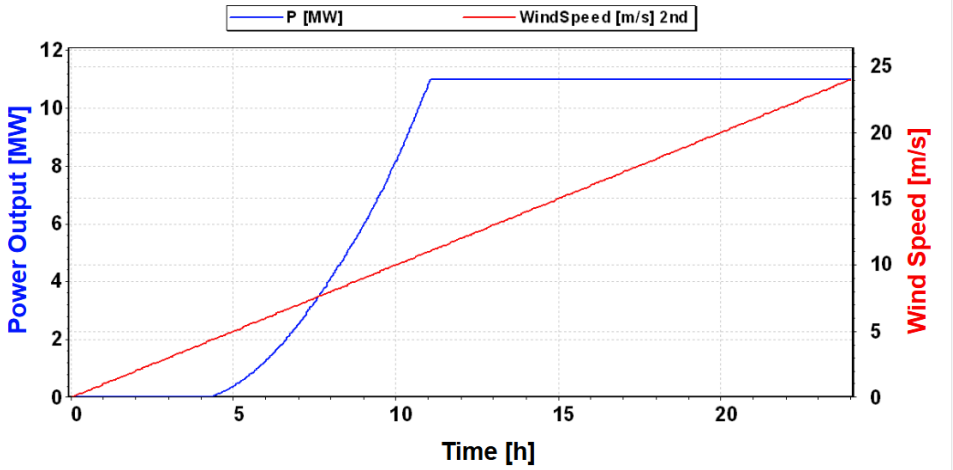

(a) Linear Increasing Wind Speeds Over 24h

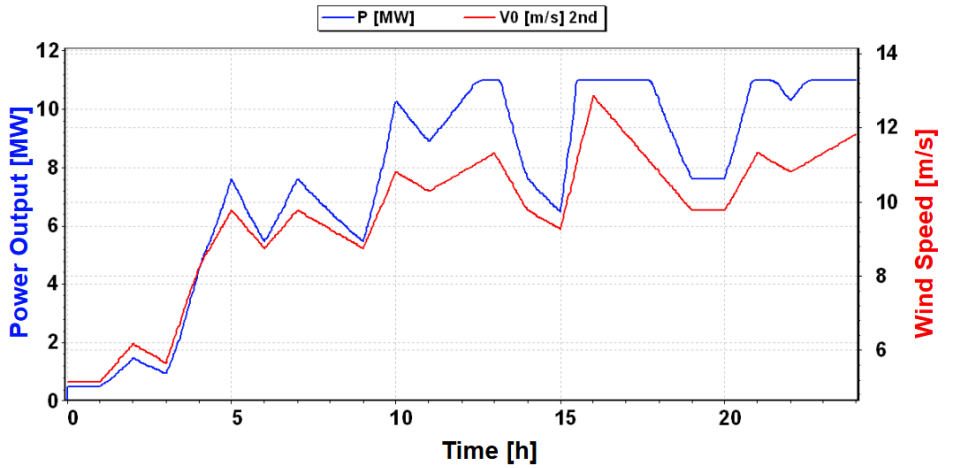

(b) Fluctuating Wind Speeds Over 24h

Figure 19: Figure (a) and (b) Show the Influence of Fluctuations in Wind Speed on the Power Output.

9.4 Effect of Inter-Turbine Distance on Velocity Deficits

This section provides insights into the velocity deficits caused by wake effects within the HKN offshore wind farm. Figure 20 shows the fluctuating wind speeds applied in both case scenarios of this research. Figure 21 shows the resulting incoming wind speeds in front of seven individual turbines, calculated using both single and multiple wake effects for a wind direction of 270° West.

The analysis compares WT10, influenced by wakes from three upstream turbines, and WT4, influenced by wakes from two upstream turbines. The velocity deficit in front of WT4 is larger than that in front of WT10, despite WT10 being affected by more upstream wakes. This is caused by the differences in spacing between the turbines, which can be seen in Figure 11 and in Appendix Table 6. These results highlight the importance of inter-turbine distances affecting the wake effects, and thereby the performance of a wind farm.

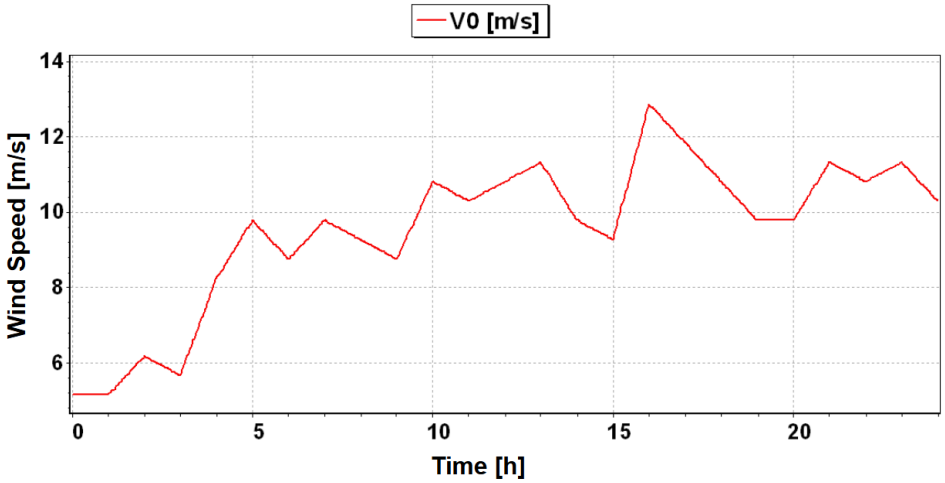

Figure 20: The Uninfluenced Wind Speeds that are Modeled for Case I and II that Characterize the Wind Speed Curve of Each Turbine that isn't Influenced by an Upstream Turbine

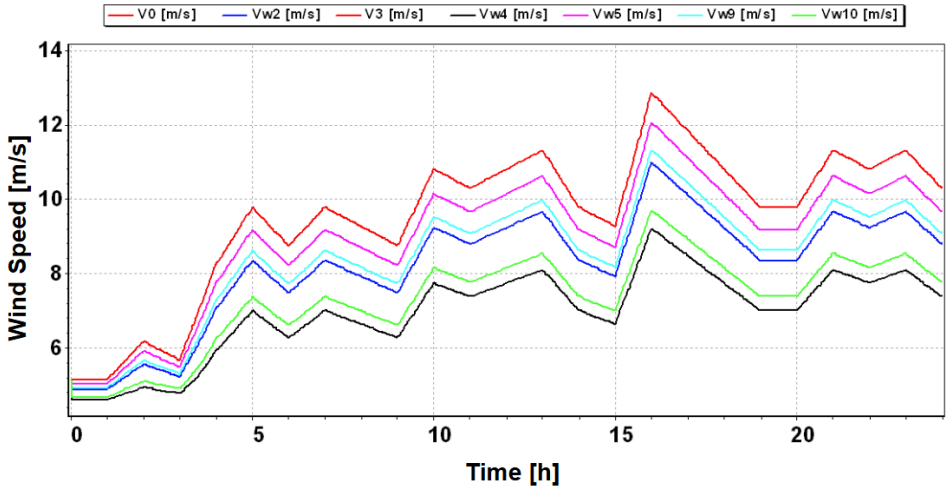

Figure 21: Wind Speeds in Front of Turbine 1 (V0), 2 (Vw2), 3 (V3), 4 (Vw4), 5 (Vw5), 9 (Vw9), and 10 (Vw10) Caused by the Single and Multiple Wake Effect of a 270° West Wind Direction

9.5 Case Scenario Results

In Figure 22 the total power output per hour is shown with influence of wake effects, together with the nominal (theoretical) power that could be produces when no wake effects are taken into account. The dotted lines represent the corresponding average power output per hour. The actual power curve led to a total energy yield of 2191 MWh with an average power output of 91 MW per hour. The nominal power curve led to a total energy yield of 3488 MWh with an average power output of 145 MW per hour. By dividing the actual energy yield by the theoretical yield an efficiency of 63 % was calculated.

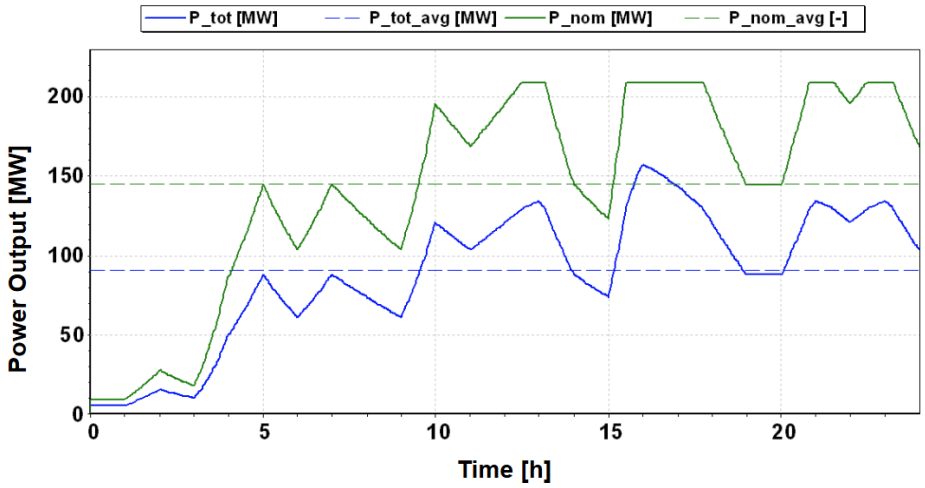

Figure 22: Case II; the Green Curve Represents the Total Nominal Power Output P_{nom} [MW] without Wake Effects and the Blue Curve the Actual Total Power Output P_{tot} [MW] With Accounting for Wake Effects

In Figure 23 the total power output per hour is shown with influence of wake effects, together with the nominal (theoretical) power that could be produces when no wake effects are taken into account. The nominal power curves are identical to the ones in Figure 22 as the same initial wind speeds are used. The dotted lines represent the corresponding average power output per hour [MW]. The actual power curve led to a total energy yield of 3110 MWh with an average power output of 130 MW per hour. The nominal power curve again led to a total energy yield of 3488 MWh with an average power output of 145 MW per hour. By dividing the actual energy yield by the theoretical yield an efficiency of 89 % was calculated, which is significantly larger than 63% obtained in case I.

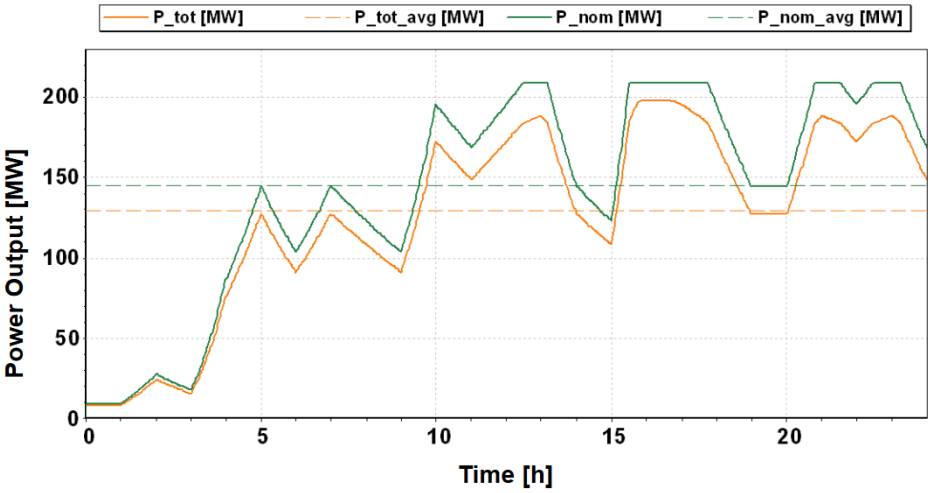

Figure 23: Case II; the Green Curve Represents the Total Nominal Power Output P_{nom} [MW] without Wake Effects and the Orange Curve the Actual Total Power Output P_{tot} [MW] With Accounting for Wake Effects

10 Model Validation

Based on existing research of a 2 MW wind turbine, a new model will be built in SIMSEN using the same formulas as presented in the article by [27]. This model serves as the basis of this research as it enables to validate the modeling approach by comparing the obtained results with the ones presented in the reference article by Saint et al. (2020) [27].

Once this model is validated, it will be expanded to represent an 11 MW wind turbine corresponding to the ones located at HKN. Previous studies have shown that a 2 MW, 5 MW, and 10 MW turbine show similar operational behavior across the different regions as explained in 4.1 [27, 54, 59]. Therefore, it is reasoned that the 11 MW turbine will show similar behavior.

To validate the 11 MW turbine model, its behavior will be compared to the patterns observed in literature sources for other turbines sizes. The main difference between the models is that parameter values, such as the cut-in wind speed, maximum power output, TSR, and rotational speed to name a few, depend on the size of the turbine. Thus graphs will align in operational behavior, but the scaled values will be different. However, a limitation of this approach is the absence of detailed 11 MW wind turbine models in literature. This indicates that the validation can't be completely confirmed. Nonetheless, the aim is to develop a model that aligns closely with actual performance.

This 11 MW turbine model will serve as the base model for modeling the HKN wind farm, where all turbines are identical. Once the single wind turbine model is complete, it will be duplicated and the spatial element between each turbine will be incorporated into the software accounting for wake effects based on the methodologies explained in Section 4.5 and 4.6, obtained from different research articles.

11 Discussion

The results of the SIMSEN models created for this research provide an approximation of the power output from the HKN wind farm, but they are unlikely to represent it fully accurately. This is due to several factors, including the simplifications and assumptions made in the current research, as well as the ongoing complexity of wind patterns and their intermittent nature. The accuracy of the model is influenced by these complexities, especially when considering how wind speed fluctuations and varying wind directions affect the wind farm's performance.

A primary challenge in the current model is the over prediction of power output, particularly due to the behavior of the power curve. The model assumes that the wind farm reaches its maximum power output before the rated wind speed is reached, which leads to an overestimation of the power produced for certain wind speeds. The different parametrization formulas for the Cp, shown in Table 8, did not solve this issue. The moment of inertia might actually affect the power curve but needs to be further investigated as the electrical domain is not accounted for in this research.

On the contrary, the assumption in Jensen's 1D model that the velocity profile expands linearly, results in over predictions of velocity deficits. This leads to an underestimation of power output. Additionally, the 1D model does not account for partial wake effects, which further leads to over predictions in velocity deficits.

Furthermore, Jensen's 1D model only considers the spatial aspect of the wake, without accounting for time delays associated with wind flows traveling downstream. The absence of these time delays leads to an under prediction of the power output as it takes time for wind flows to travel downstream. Adding this delay is crucial for more accurate predictions of energy production, which is not captured by the 1D approach.

On the other hand, the more advanced 2D wake models include a two-dimensional wake expansion by which partial wakes are captured and more accurate velocity predictions can be obtained. Among the 2D wake models discussed in Section 4.4, the Jensen-Gaussian 2D model was found to be most accurate. Adding the extensions of Jensen-Gaussian to the 1D model allows for more accurate performance prediction of HKN under varying conditions.

From the model results in Section 9 it was found that fluctuating wind speeds and wind directions have a significant impact on the power output. Even small variations in wind speed directly cause the power curve to change, which highlights the sensitivity of wind farm performance influences by wind fluctuations.

Wind fluctuations can be easily integrated into the model using forecast data, with the wind turbines adjusting their behavior based on wind speeds. This forecast data can be quickly modified via a lookup table in the model. However, wind directions present a more significant challenge, as the distances between turbines are currently calculated manually. This process is time-consuming and difficult to adapt quickly, making the modification of wind directions more complex compared to wind speed adjustments. While the manual calculation provides an accurate estimation, further improvements in this area could enhance the model's accuracy.

The impact of wind direction is particularly important, as proven in Figures 22 and 23. Namely, the efficiency of the wind farm is highly sensitive to the incoming wind direction. When the wind comes from a 270° direction, the total efficiency of the wind farm drops to 63%, while the efficiency increases to 89% when wind comes from a 225° SW direction. This highlights that the wind direction plays a crucial role in wind farm layout optimization.

The wind rose in Figure 10 shows that, in the HKN area, winds typically come from the SSW

and WSW directions. Therefore, optimizing the wind farm layout to minimize wake effects from these directions is essential for maximizing energy yield. The results from this study confirm that this consideration has been effectively addressed, as the SW direction (representing the average of the SSW and WSW) leads to a significantly higher energy yield than the West direction.

To sum up all points made above, while the current results provide useful insights into the power output of the HKN wind farm, there are several limitations that need to be addressed in future studies. These include, refining the modeling of wake effects in terms of adding time delays and exploring the potential of more advanced 2D wake models such as Jensen-Gaussian, which also include partial wakes. Additionally, optimizing the wind farm layout based on wind direction and minimizing wake effects will play a significant role in improving overall efficiency. Last, the current model shows promising results, indicating its potential for accurate performance prediction. However, it remains a simplified representation and requires further refinement and validation in future research. Particular attention should be given to reviewing the assumptions outlined in Section 8, as these play a critical role in influencing the model's outcomes and may need adjustment for improved accuracy and applicability.

12 Conclusion

This research developed and tested a model of the HKN offshore wind farm in SIMSEN, simulating energy production and wake effects under site-specific wind conditions. The model provided an approximation of the wind farm's power output and successfully included fluctuating wind speeds using lookup tables based on forecast data. This method allows for the effects of wind speed variability on turbine performance to be simulated accurately.

However, there are still challenges, especially when it comes to modeling fluctuating wind directions. This study analyzed two constant wind directions (270° W and 225° SW) and found that changes in wind direction significantly influence power output due to varying wake effects. Currently, the inter-turbine distances for different wind directions are calculated manually, which makes it difficult to analyze directional variability efficiently. Automating these calculations would improve the model and enhance the computational efficiency of evaluating the impact of changing wind directions on wind farm performance.

The current model also has limitations due to simplifications. For example, assumptions in Jensen's 1D wake model lead to over predictions of velocity deficits, which result in underestimating power output. Furthermore, the model does not account for time delays associated with wakes traveling downstream, which affects the accuracy of energy production predictions. Advanced wake models, such as the Jensen-Gaussian 2D model, provide more accurate results by including partial wakes and two-dimensional wake expansions. Adding these features and accounting for time delays would improve the model significantly.

This study also showed the importance of optimizing wind farm layouts to reduce wake effects from the most common wind directions. The wind rose for the HKN site shows that winds typically come from the SSW and WSW directions. Results revealed that the efficiency of the wind farm drops to 63% when the wind comes from 270° W, compared to 89% when it comes from 225° SW. This demonstrates that optimizing the layout for the dominant wind directions is crucial for maximizing energy production for future offshore wind farms.

In conclusion, this research addressed the main question introduced in Section **??**: How can the HKN offshore wind farm be modeled in SIMSEN to assess wake effects and turbine performance under site-specific wind conditions, including fluctuating wind speeds and directions, for accurate performance prediction? While this research provides valuable insights, there are still opportunities for refinement. Future work should focus on refining wake modeling by integrating more advanced 2D wake models, automating calculations for changing wind directions, and addressing the assumptions outlined in Section 8. These enhancements would increase the accuracy and reliability of the model. By addressing these challenges, future research could further support the integration of energy storage systems and contribute to the stability and efficiency of renewable energy systems.

Bibliography

[1] Government of the Netherlands, "Step by step, the netherlands is transitioning to sustainable energy," n.d., accessed: 2024-12-02. [Online]. Available: https://www.government.nl/topics/renewable-energy/step-by-step-the-netherlands-is-transitioning-to-sustainable-energy

[2] I. E. Agency, "Wind energy," https://www.iea.org/energy-system/renewables/wind, 2024, accessed: 2024-10-13.

[3] N. Mlilo, J. Brown, and T. Ahfock, "Impact of intermittent renewable energy generation penetration on the power system networks–a review," *Technology and Economics of Smart Grids and Sustainable Energy*, vol. 6, no. 1, p. 25, 2021.

[4] I. E. Agency, "World energy outlook 2022 - key findings," https://www.iea.org/reports/world-energy-outlook-2022/key-findings, 2022, accessed: 2024-10-13.

[5] M. Y. Suberu, M. W. Mustafa, and N. Bashir, "Energy storage systems for renewable energy power sector integration and mitigation of intermittency," *Renewable and Sustainable Energy Reviews*, vol. 35, pp. 499–514, 2014.

[6] O. Grazer, "Utility-scale energy storage," https://oceangrazer.com/utility-scale-energy-storage/, 2025, accessed: 2025-01-15.

[7] D. A. Elalfy, E. Gouda, M. F. Kotb, V. Bureš, and B. E. Sedhom, "Comprehensive review of energy storage systems technologies, objectives, challenges, and future trends," *Energy Strategy Reviews*, vol. 54, p. 101482, 2024.

[8] Energy Technology Data Exchange (ETDE), "Offshore wind energy: technology, policy, and project management," 2008, accessed: 2024-12-02. [Online]. Available: https://www.osti.gov/etdeweb/servlets/purl/945121

[9] K. Yang, G. Kwak, K. Cho, and J. Huh, "Wind farm layout optimization for wake effect uniformity," *Energy*, vol. 183, pp. 983–995, 2019.

[10] A. E. Dinçer, A. Demir, and K. Yılmaz, "Multi-objective turbine allocation on a wind farm site," *Applied Energy*, vol. 355, p. 122346, 2024.

[11] Y.-K. Wu, W.-C. Wu, and J.-J. Zeng, "Key issues on the design of an offshore wind farm layout and its equivalent model," *Applied Sciences*, vol. 9, no. 9, p. 1911, 2019.

[12] C. Nicolet, A. Beguin, B. Kawkabani, Y. Pannatier, A. Schwery, and F. Avellan, "Variable speed and ternary units to mitigate wind and solar intermittent production," *Hydro Vision*, 2014.

[13] Power Vision Engineering, "Company," 2024, accessed: 2024-10-10. [Online]. Available: https://powervision-eng.ch/company/

[14] D. Petković, Ž. Ćojbašič, and V. Nikolić, "Adaptive neuro-fuzzy approach for wind turbine power coefficient estimation," *Renewable and Sustainable Energy Reviews*, vol. 28, pp. 191–195, 2013.

[15] A. Chaudhuri, R. Datta, M. P. Kumar, J. P. Davim, and S. Pramanik, "Energy conversion strategies for wind energy system: Electrical, mechanical and material aspects," *Materials*, vol. 15, no. 3, p. 1232, 2022.

[16] Y. Dong, G. Tang, Y. Jia, Z. Wang, X. Rong, C. Cai, Q. Li, and Y. Yang, "Review on research about wake effects of offshore wind turbines," *Energy Engineering*, vol. 119, no. 4, pp. 1341–1360, 2022.

[17] T. Göçmen, P. Van der Laan, P.-E. Réthoré, A. P. Diaz, G. C. Larsen, and S. Ott, "Wind turbine wake models developed at the technical university of denmark: A review," *Renewable and Sustainable Energy Reviews*, vol. 60, pp. 752–769, 2016.

[18] Z. Shao, Y. Wu, L. Li, S. Han, and Y. Liu, "Multiple wind turbine wakes modeling considering the faster wake recovery in overlapped wakes," *Energies*, vol. 12, no. 4, p. 680, 2019.

[19] C. L. Archer, A. Vasel-Be-Hagh, C. Yan, S. Wu, Y. Pan, J. F. Brodie, and A. E. Maguire, "Review and evaluation of wake loss models for wind energy applications," *Applied Energy*, vol. 226, pp. 1187–1207, 2018.

[20] R. Shakoor, M. Y. Hassan, A. Raheem, and Y.-K. Wu, "Wake effect modeling: A review of wind farm layout optimization using jensen s model," *Renewable and Sustainable Energy Reviews*, vol. 58, pp. 1048–1059, 2016.

[21] X. Gao, K. Zhou, R. Liu, W. Ma, X. Gong, X. Zhu, Y. Wang, and F. Zhao, "Aerodynamic characteristics of wind turbines considering the inhomogeneity and periodic incentive of wake effects," *Energy*, vol. 310, p. 133275, 2024.

[22] M. Wang, M. Zhang, L. Zhao, and C. Qin, "A wake prediction framework based on the most gaussian wake model and a deep learning approach," *Journal of Wind Engineering and Industrial Aerodynamics*, vol. 255, p. 105952, 2024.

[23] Windfinder, "Windfinder - weather forecast," 2024, accessed: 2024-12-23. [Online]. Available: https://nl.windfinder.com/#13/52.6189/4.6280/sfc/2024-12-19T10:00Z/report

[24] PowerVision, "Simsen software," https://powervision-eng.ch/simsen-software/, 2023, accessed: 2024-10-09.

[25] National Instruments, "Wind turbine control methods," n.d., accessed: 2025-01-16. [Online]. Available: https://www.ni.com/en/solutions/energy/wind-turbine-control-methods.html

[26] W.-S. D. Team, "Wec-sim: Wave energy converter simulator - theory documentation," 2024, accessed: 2024-12-04. [Online]. Available: https://wec-sim.github.io/WEC-Sim/main/most/theory.html

[27] Y.-M. Saint-Drenan, R. Besseau, M. Jansen, I. Staffell, A. Troccoli, L. Dubus, J. Schmidt, K. Gruber, S. G. Simões, and S. Heier, "A parametric model for wind turbine power curves incorporating environmental conditions," *Renewable Energy*, vol. 157, pp. 754–768, 2020.

[28] P. C. Rocha, J. C. de Araujo, R. P. Lima, M. V. da Silva, D. Albiero, C. de Andrade, and F. Carneiro, "The effects of blade pitch angle on the performance of small-scale wind turbine in urban environments," *Energy*, vol. 148, pp. 169–178, 2018.

[29] I. Neunaber, M. Hölling, and M. Obligado, "Leading effect for wind turbine wake models," *Renewable Energy*, vol. 223, p. 119935, 2024.

[30] L. Parada, C. Herrera, P. Flores, and V. Parada, "Wind farm layout optimization using a gaussian-based wake model," *Renewable energy*, vol. 107, pp. 531–541, 2017.

[31] S. Tao, Q. Xu, A. Feijóo, G. Zheng, and J. Zhou, "Nonuniform wind farm layout optimization: A state-of-the-art review," *Energy*, vol. 209, p. 118339, 2020.

[32] M. Ertan, O. Koşar, and M. A. Özgür, "A comparison of an analytic gaussian wake model with a classical model for wind farm layout optimization," in *International Symposium on Energy Management and Sustainability*. Springer, 2022, pp. 577–585.

[33] P. Hou, J. Zhu, K. Ma, G. Yang, W. Hu, and Z. Chen, "A review of offshore wind farm layout optimization and electrical system design methods," *Journal of Modern Power Systems and Clean Energy*, vol. 7, no. 5, pp. 975–986, 2019.

[34] Y. Wu, Y. Cao, Z. Chen, Y. Xue, K. Sun, Y. Xu, F. Wang, and X. Zhou, "Key technologies and research directions of wind power generation in the 21st century: A review," *Journal of Modern Power Systems and Clean Energy*, vol. 7, no. 1, pp. 1–15, January 2019. [Online]. Available: https://link.springer.com/article/10.1007/s40565-019-0550-5

[35] L. Tian, W. Zhu, W. Shen, N. Zhao, and Z. Shen, "Development and validation of a new two-dimensional wake model for wind turbine wakes," *Journal of Wind Engineering and Industrial Aerodynamics*, vol. 137, pp. 90–99, 2015.

[36] L. Tian, W. Zhu, W. Shen, Y. Song, and N. Zhao, "Prediction of multi-wake problems using an improved jensen wake model," *Renewable energy*, vol. 102, pp. 457–469, 2017.

[37] X. Gao, Y. Li, F. Zhao, and H. Sun, "Comparisons of the accuracy of different wake models in wind farm layout optimization," *Energy Exploration & Exploitation*, vol. 38, no. 5, pp. 1725–1741, 2020.

[38] N. Moskalenko, K. Rudion, and A. Orths, "Study of wake effects for offshore wind farm planning," in *2010 Modern Electric Power Systems*. IEEE, 2010, pp. 1–7.

[39] R. Asfour, T. Brahimi, and M. El-Amin, "Wind farm layout: modeling and optimization using genetic algorithm," in *IOP Conference Series: Earth and Environmental Science*, vol. 1008, no. 1. IOP Publishing, 2022, p. 012004.

[40] Simsen Help Desk, *Wind Farm Block in Simsen*, Power Vision Engineering, 2024, accessed from local file: WindFarm_Block_Simsen.pdf.

[41] V. Reyes, J. J. Rodríguez, O. Carranza, and R. Ortega, "Review of mathematical models of both the power coefficient and the torque coefficient in wind turbines," in *2015 IEEE 24th international symposium on industrial electronics (ISIE)*. IEEE, 2015, pp. 1458–1463.

[42] A. W. Manyonge, R. Ochieng, F. Onyango, and J. Shichikha, "Mathematical modelling of wind turbine in a wind energy conversion system: Power coefficient analysis," 2012.

[43] M. Ragheb and A. M. Ragheb, "Wind turbines theory-the betz equation and optimal rotor tip speed ratio," *Fundamental and advanced topics in wind power*, vol. 1, no. 1, pp. 19–38, 2011.

[44] W. H. A. Lio, *Blade-pitch control for wind turbine load reductions*. Springer, 2018.

[45] T. Burton, N. Jenkins, D. Sharpe, and E. Bossanyi, *Wind Energy Handbook*, second edition ed. Chichester, UK: John Wiley & Sons, Ltd., 2011.

[46] W. P. Plus, "Betz's law," 2022, accessed: 2025-01-12. [Online]. Available: https://windpowerplus.com/betzs-law/

[47] T. Burton, N. Jenkins, E. Bossanyi, and D. Sharpe, *Wind Energy Handbook*, 3rd ed. Chichester, UK: Wiley, 2021. [Online]. Available: https://www.wiley.com/en-us/Wind+Energy+Handbook%2C+3rd+Edition-p-9781119472910

[48] GeoGebra, "Geogebra classic," 2024, accessed: 2024-12-26. [Online]. Available: https://www.geogebra.org/classic?lang=nl

[49] Ministerie van Infrastructuur en Waterstaat, "Windenergiegebied hollandse kust (noord) inclusief prinses amalia windpark (pawp)," 2023, accessed: 2023-12-23. [Online]. Available: https://www.noordzeeloket.nl/functies-gebruik/windenergie/doorvaart-medegebruik/hollandse-kust-noord-inclusief-prinses-amalia/

[50] CrossWind, "Wind farm – crosswind hollandse kust noord," n.d., accessed: 2024-12-04. [Online]. Available: https://www.crosswindhkn.nl/windfarm/

[51] Siemens Gamesa Renewable Energy, "Siemens Gamesa SG 11.0-200 DD," https://en.wind-turbine-models.com/turbines/2157-siemens-gamesa-sg-11.0-200-dd, n.d., accessed: 2024-12-27. [Online]. Available: https://en.wind-turbine-models.com/turbines/2157-siemens-gamesa-sg-11.0-200-dd

[52] E. part of TNO, "Scoping analysis of the potential yield of the hollandse kust (noord) wind farm and the influence on the existing wind farms in the proximity," ECN part of TNO, Tech. Rep., 2018, accessed: 30-12-2024. [Online]. Available: https://energy.nl/wp-content/uploads/ecn-e-18-033-3.pdf

[53] J. Liew, G. R. Pirrung, and A. M. Urbán, "Effect of varying fidelity turbine models on wake loss prediction," in *Journal of Physics: Conference Series*, vol. 1618, no. 6. IOP Publishing, 2020, p. 062002.

[54] IEA Wind TCP Task 37, "Systems engineering in wind energy - wp2.1 reference wind turbines," IEA Wind TCP, Technical Report, May 2019.

[55] Siemens Gamesa, "Siemens gamesa sg 11.0-200 dd," 2023, accessed: 2025-01-08. [Online]. Available: https://en.wind-turbine-models.com/turbines/2157-siemens-gamesa-sg-11.0-200-dd

[56] C. Bak, "The dtu 10mw reference turbine," Technical University of Denmark (DTU), Tech. Rep., 2017. [Online]. Available: https://backend.orbit.dtu.dk/ws/portalfiles/portal/55645274/The_DTU_10MW_Reference_Turbine_Christian_Bak.pdf

[57] S. Zergane, C. Farsi, S. Amroune, S. Benkherbache, and N. Menasri, "A new study on the effect of the partial wake generated in a wind farm," *Energies*, vol. 17, no. 6, p. 1498, 2024.

[58] G. Dong, Z. Li, J. Qin, and X. Yang, "How far the wake of a wind farm can persist for?" *Theoretical and Applied Mechanics Letters*, vol. 12, no. 1, p. 100314, 2022.

[59] J. Jonkman, S. Butterfield, W. Musial, and G. Scott, "Definition of a 5-mw reference wind turbine for offshore system development," National Renewable Energy Laboratory (NREL), Technical Report NREL/TP-500-38060, Feb. 2009. [Online]. Available: https://www.nrel.gov/docs/fy09osti/38060.pdf

1 Appendix

1.1 Case Data

Table 5: Wind Speed Data of a Regular Day in December 2024 in Knots, Meters per Second, and Corresponding Wind Direction [48]

Time [h]	$C_{\mathbf{inf}}$ **[kts]**	$C_{\mathbf{inf}}$ **[m/s]**	**Wind Direction [deg]**
0	10	5.144	302
1	10	5.144	301
2	12	6.173	298
3	11	5.659	292
4	16	8.231	279
5	19	9.774	268
6	17	8.746	257
7	19	9.774	253
8	18	9.260	249
9	17	8.746	250
10	21	10.803	249
11	20	10.289	267
12	21	10.803	270
13	22	11.318	264
14	19	9.774	272
15	18	9.260	271
16	25	12.861	267
17	23	11.832	264
18	21	10.803	261
19	19	9.774	258
20	19	9.774	257
21	22	11.318	254
22	21	10.803	254
23	22	11.318	261
24	20	10.289	261

Table 6 and 7 present the inter-turbine spaces between downstream turbines affected by the wakes of upstream turbines. x_{scale} represents the distance on the map created in GeoGebra and x_{actual} represents the actual distance between the turbines at HKN.

Table 6: Inter-spaces Between Wind Turbines Experiencing Wake Effects From Upstream Wind Turbines Case I (270 degrees)

Upstream - Downstream WT No.	$x_{\mathbf{scale}}$ [-]	$x_{\mathbf{actual}}$ [m]
1 - 2	0.3224	1031.68
1 - 4	0.645	2064
2 - 4	0.3226	1032.32
3 - 5	0.9155	2929.6
6 - 8	1.3792	4413.44
3 - 9	1.83969	5887.008
5 - 9	0.92419	2957.408
3 - 10	2.18886	7004.352
5 - 10	1.27336	4074.752
9 - 10	0.34917	1117.344
3 - 11	2.5473	8151.36
5 - 11	1.6318	5221.76
9 - 11	0.70761	2264.352
10 - 11	0.35844	1147.008
3 - 12	2.90043	9281.376
5 - 12	1.98493	6351.776
10 - 12	0.71157	2277.024
11 - 12	0.35313	1130.016
14 - 15	0.53824	1722.368
15 - 16	0.54532	1745.024
13 - 17	1.73228	5543.296
16 - 17	0.54662	1749.184
13 - 18	2.2743	7277.76
17 - 18	0.54202	1734.464
7 - 19	2.15082	6882.624
13 - 19	2.8145	9006.4
18 - 19	0.5402	1728.64

Table 7: Inter-spaces Between Wind Turbines Experiencing Wake Effects From Upstream Wind Turbines Case II (225 degrees)

Upstream - Downstream WT No.	$x_{\mathbf{scale}}$ [-]	$x_{\mathbf{actual}}$ [m]
2 - 7	0.88	2816
3 - 15	1.12	3584
2 - 16	1.47	4704
4 - 16	1.22	3904
5 - 16	0.83	2656
8 - 17	0.57	1824
9 - 18	0.87	2784
11 - 19	0.65	2080

1.2 Power Coefficient Exponential Model Parameters

Table 8: Comparison of Cp Coefficients from Different sources [27]

Coefficient	**Slootweg et al. (2001, 2003)**	**Heier (2014)**	**Thongam et al. (2009)**	**De Kooning et al. (2013)**	**Ochieng et al. (2014)**	**Dai et al. (2016)**
c_1	0.73	0.5	0.5176	0.77	0.5	0.22
c_2	151	116	116	151	116	120
c_3	0.58	0.4	0.4	0	0	0.4
c_4	0	0	0	0	0.4	0
c_5	0.002	0	0	0	0	0
x	2.14	0	0	0	0	0
c_6	13.2	5	5	13.65	5	5
c_7	18.4	21	21	18.4	21	12.5
c_8	0	0	0.006795	0	0	0
c_9	-0.02	0.089	0.089	0	0.08	0.08
c_{10}	0.003	0.035	0.035	0	0.035	0.035

1.3 Axial Induction Factor a

Table 9: Solutions for axial induction factor a [-] obtained by solving Equation 23 for every Cp value

Cinf [m/s]	Cp [-]	a_1 [-]	a_2 [-]	a_3 [-]
0.0	0.000	0.000	1.000	-
1.0	0.000	0.000	1.000	-
2.0	0.000	0.000	1.000	-
3.0	0.000	0.000	1.000	-
4.0	0.000	0.000	1.000	-
4.2	0.000	0.000	1.000	-
4.5	0.062	0.016	0.86623	1.11775
5.0	0.168	0.04616	0.76581	1.18802
6.0	0.310	0.09452	0.65638	1.24908
7.0	0.386	0.12646	0.59843	1.2751
8.0	0.420	0.14294	0.57128	1.28576
9.0	0.425	0.14552	0.56718	1.28729
10.0	0.425	0.14552	0.56718	1.28729
11.0	0.425	0.14552	0.56718	1.28729
12.0	0.425	0.14552	0.56718	1.28729
13.0	0.425	0.14552	0.56718	1.28729
14.0	0.425	0.14552	0.56718	1.28729
15.0	0.351	0.11104	0.62542	1.26353
16.0	0.314	0.09607	0.65338	1.25054
17.0	0.288	0.08623	0.67288	1.24088
18.0	0.268	0.07898	0.68791	1.23309
19.0	0.251	0.07302	0.70075	1.22621
20.0	0.237	0.06824	0.7114	1.22034
21.0	0.224	0.0639	0.72138	1.21471
22.0	0.213	0.0603	0.72989	1.20979
23.0	0.202	0.05676	0.7385	1.20473
24.0	0.192	0.05358	0.74641	1.20000
25.0	0.183	0.05077	0.75361	1.19561
26.0	0.175	0.0483	0.76008	1.19161
27.0	0.167	0.04585	0.76663	1.18750
28.0	0.158	0.04314	0.7741	1.18274
29.0	0.150	0.04075	0.78085	1.17839
30.0	0.143	0.03868	0.78684	1.17446
31.0	0.135	0.03634	0.7938	1.16985
32.0	0.127	0.03402	0.80089	1.16507
32.0	0.000	0.000	1.000	-

1.4 Pitch Angle Lookup Table

Table 10: Wind Velocity and Corresponding Pitch Angles for an 11 MW Wind Turbine

Wind Velocity (m/s)	**Pitch Angle (deg)**
1	0.000
2	0.000
3	0.000
4	0.000
5	0.000
6	0.000
7	0.000
8	0.000
9	0.000
10	0.000
11	0.000
12	0.000
13	0.000
14	0.000
14.5	2.633
15	4.537
15.5	5.975
16.5	8.250
17.5	10.121
18.5	11.771
19.5	13.280
21.5	16.018
23.5	18.513
28.5	24.110